Catalysis Today 436 (2024) 114725

Contents lists available at ScienceDirect

Catalysis Today

journal homepage: www.elsevier.com/locate/cattod

TiO_2 nanotubes immobilized on polyurethane foam as a floating photocatalyst for water treatment

Nila Davari [a], Ermelinda Falletta [b,c], Claudia L. Bianchi [b,c], Viviane Yargeau [d], Daria C. Boffito [a,e,*]

[a] Department of Chemical Engineering, Polytechnique Montréal, Montréal, Canada
[b] Department of Chemistry, University of Milan, Milan, Italy
[c] Consorzio Interuniversitario Nazionale per la Scienza e Tecnologia dei Materiali (INSTM), via Giusti 9, Florence 50121, Italy
[d] Department of Chemical Engineering, McGill University, Montréal, Canada
[e] Canada Research Chair in Engineering Process Intensification and Catalysis, Canada

ARTICLE INFO

Keywords:
Photocatalyst
Floating TiO_2 nanoparticles
Floating TiO_2 nanotubes
PU Foam
Bisphenol A
Sunlight

ABSTRACT

We investigated the photocatalytic activity of TiO_2 nanoparticles (TiO_2-NPs) and TiO_2 nanotubes (TiO_2-NTs) supported on a floating polyurethane (PU) foam for removing Bisphenol A (BPA) as a model pollutant. We fabricated TiO_2-NPs by the sol-gel method and TiO_2-NTs by the ultrasound-assisted hydrothermal method. Subsequently, the photocatalysts were immobilized onto the PU foam through the wet chemical deposition process. The synthesized photocatalysts were characterized by contact angle, SEM-EDS, TEM, XRD, DRS, and BET analyses. TiO_2-NPs and TiO_2-NTs were successfully deposited onto the PU foam, creating floating photocatalysts denoted as TiO_2-NPs@PU and TiO_2-NTs@PU. Our findings indicated that the nanotubular structure of floating TiO_2 photocatalysts enhanced the removal efficiency of BPA relative to the nanoparticles, resulting in the complete removal of the pollutant over 180 min of simulated sunlight irradiation. TiO_2-NTs@PU was also stable after five reuse cycles. Moreover, h^+ was the main scavenging reactive species during the photocatalysis of BPA with TiO_2-NTs@PU.

1. Introduction

The application of TiO_2 semiconductors has been investigated in solar cells, fuel cells, Li-ion batteries, H_2 production, air purification, CO_2 conversion, NO_x gases conversion, heavy metals reduction, gas sensors, water splitting, and especially wastewater treatment with photocatalytic processes [1,2]. Photocatalysis by TiO_2 that mimics artificial photosynthesis employs TiO_2 semiconductors as photocatalysts for light-driven photocatalytic removal of hazardous organic pollutants from wastewater [3,4].

TiO_2 photocatalysts have drawn attention due to their characteristics, including hydrophilicity, thermal and chemical stability, optical properties, corrosion resistance, and photocatalytic activity under light irradiation [5–8].

However, TiO_2 has limitations originating from the low electron transfer rate and light absorption, as well as the rapid recombination of photogenerated electron-hole pairs in the photocatalyst. Furthermore, employing TiO_2 in the powder format is another obstacle, making TiO_2 recovery challenging after the photocatalytic process [9,10].

To modify the photocatalytic activity of TiO_2, TiO_2 nanostructures can be engineered into nanotubes, which results in enhanced electron migration and reduced electron-hole recombination [11–13]. TiO_2 nanotubes (TiO_2-NTs) have a large surface area, higher light absorption, and oriented charge mobility in comparison to TiO_2 nanoparticles (TiO_2-NPs) [14,15]. Several research has been reported on the synthesis of TiO_2-NTs photocatalysts, including the template-assisted method, sol-gel process, electrochemical anodization of titanium, and hydrothermal method [16,17]. Among these methods, hydrothermal is a common approach to converting TiO_2 powder as a precursor to the 1D nanotubular structure (TiO_2-NTs) [17].

Floating TiO_2 photocatalysts can be considered a promising approach to tackle the recovery and reusability issues of suspended ones and prevent environmental toxicity from releasing nanoparticles to treated water. Compared with suspended systems, floating TiO_2 photocatalysts can benefit from more accessibility to the water-air interface, resulting in better solar light harnessing. This can boost the removal

* Corresponding author at: Department of Chemical Engineering, Polytechnique Montréal, Montréal, Canada.
E-mail address: daria-camilla.boffito@polymtl.ca (D.C. Boffito).

https://doi.org/10.1016/j.cattod.2024.114725
Received 30 October 2023; Received in revised form 3 April 2024; Accepted 13 April 2024
Available online 15 April 2024
0920-5861/© 2024 The Authors. Published by Elsevier B.V. This is an open access article under the CC BY-NC license (http://creativecommons.org/licenses/by-nc/4.0/).

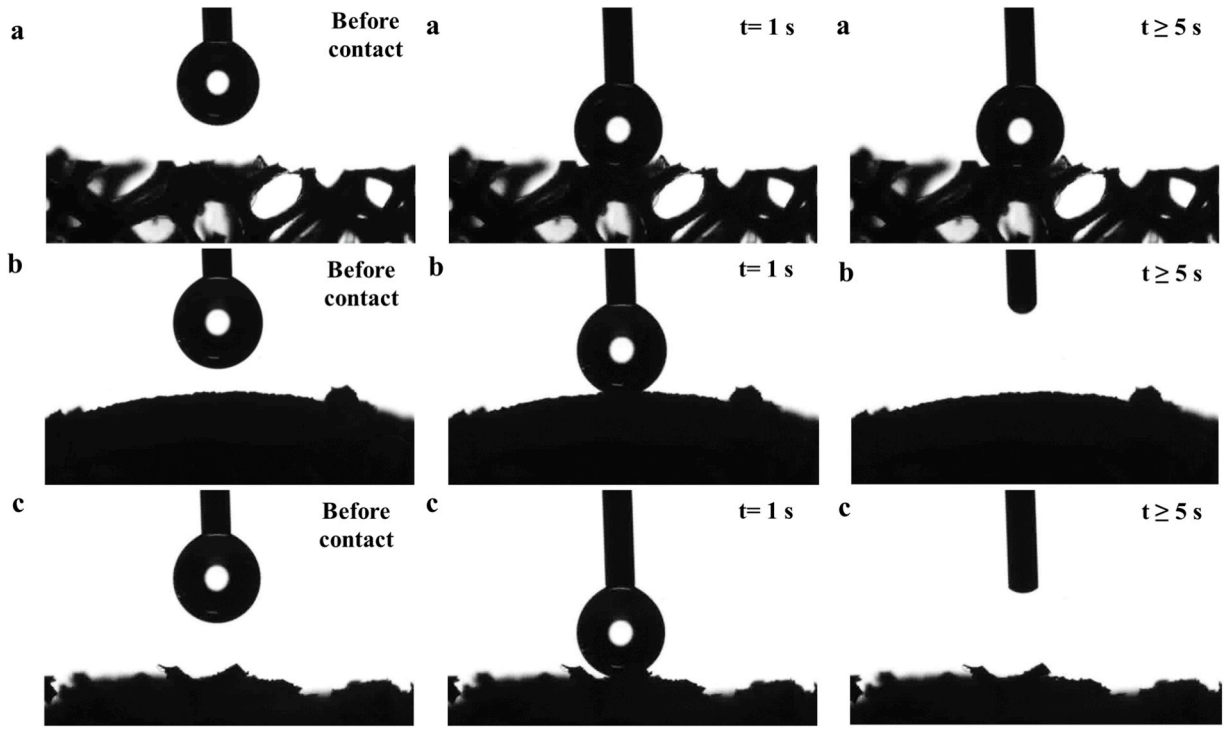

Fig. 1. Dynamic water contact angle for (a) pristine PU foam, (b) TiO_2-NPs@PU, and (c) TiO_2-NTs@PU.

efficiency of contaminants from wastewater [18–21].

Floating substrates, including perlite, vermiculite, glass microbead, cork, graphite, polymer, light-expanded clay aggregate, silicone, and autoclaved cellular concrete, have been employed in immobilized floating TiO_2-based photocatalysts for water purification [22]. Polyurethane (PU) foam is a macroporous polymer with a three-dimensional structure. The open-pore structure of the PU foam increases porosity and surface area, which improves the adsorption ability of pollutants. Therefore, the removal efficiency of aqueous contaminants can be enhanced [23,24]. In addition, PU foam has low density (< 1000 kg/m^3), making it a suitable floating support [25]. According to the literature, Zhang et al. [24] synthesized well-ordered mesoporous TiO_2 photocatalysts onto floating PU foam. Based on the results, the heavy metal ions in the mixed solution were completely removed, and the removal efficiency of the dye was greater than 90% under sunlight irradiation after 2 h. Zhang et al. [26] described preparing ordered mesoporous SiO_2-TiO_2 photocatalysts based on a PU foam. Floating SiO_2-TiO_2/PUF photocatalyst was applied in a photocatalytic circulating-bed biofilm reactor where phenol and 2,4,5-trichlorophenol were completely removed under 3 h and 6 h of UV irradiation (365 nm, 8 W), respectively. Ni et al. [23] fabricated floating photocatalysts based on polyurethane foams with Ag/TiO_2/graphene nanoparticles. The photocatalytic activity of floating PU-Ag/TiO_2/graphene was investigated for diesel degradation under visible light irradiation (500 W, Halogen tungsten lamp). The results reported 76% of diesel degradation during 16 h. In another study, Li et al. [18] synthesized a floating photocatalyst, which was TiO_2 P25 nanoparticles supported on a polyurethane foam to degrade BPA. The degradation efficiency with TiO_2 P25/PU was achieved at 71% after 120 min UV irradiation.

To the best of our knowledge, no study has been reported to remove pollutants from wastewater using mesoporous TiO_2-NTs photocatalysts immobilized on a macroporous PU foam as a floating macro/mesoporous photocatalyst carrier. Herein, we investigated for the first time the photocatalytic performance of the floating nanocomposite foam (TiO_2-NTs@PU) to eliminate Bisphenol A (BPA), a model organic pollutant in wastewater, when exposed to simulated solar irradiation. In addition, this work was the first to report the effect of the nanotubular structure of TiO_2 on the activity of floating TiO_2 photocatalysts in degrading BPA under simulated sunlight. Furthermore, the mechanism of BPA degradation with floating TiO_2-NTs@PU was examined by capturing free radical species.

2. Materials and methods

2.1. Chemicals

We used Ti(IV)-butoxide ($C_{16}H_{36}O_4Ti$, reagent grade, 97%, Sigma Aldrich), Ethanol (C_2H_6O, 95%, Commercial Alcohols), Sodium hydroxide (NaOH, 98%, Thermo Scientific), Hydrochloric acid (HCl, 37% w/w, Fisher Scientific), Polyvinyl alcohol (low molecular weight, 98–99% hydrolyzed, Thermo Scientific Chemicals), Bisphenol A (≥99%, Sigma Aldrich), and DMPO (5,5-Dimethyl-1-pyrroline N-oxide, Sigma-Aldrich). Porous Polyurethane foam (Porosity: Medium, 20 PPI) was purchased from Amtra. We prepared all solutions with deionized water.

2.2. Fabrication of photocatalysts

2.2.1. TiO_2-NPs

We synthesized TiO_2-NPs by the sol-gel method [27]. First, we mixed $C_{16}H_{36}O_4Ti$ (25 mL) and ethanol (80 mL) for 4 h at 25 °C with a magnetic stirrer. After that, we kept the solution for aging for 12 h at room temperature. The sample was then dried at 80 °C in an oven and calcined in a furnace at 400 °C for 2 h (heating rate of 5 °C/min under air atmosphere).

2.2.2. TiO_2-NTs

We synthesized TiO_2-NTs by the ultrasound-assisted hydrothermal method [28]. First, we added the previously synthesized TiO_2-NPs (1 g) to NaOH solution (10 M, 50 mL) under 30 min stirring at room temperature to make a suspension. To homogenize the suspension, the sample was then kept under ultrasonication (110 W, 30 min). Afterwards, the homogenized suspension was transferred into a Teflon-lined autoclave (100 mL), heated to 160 °C with a heating rate of 5 °C/min and maintained for 24 h in an oven. After cooling to room temperature,

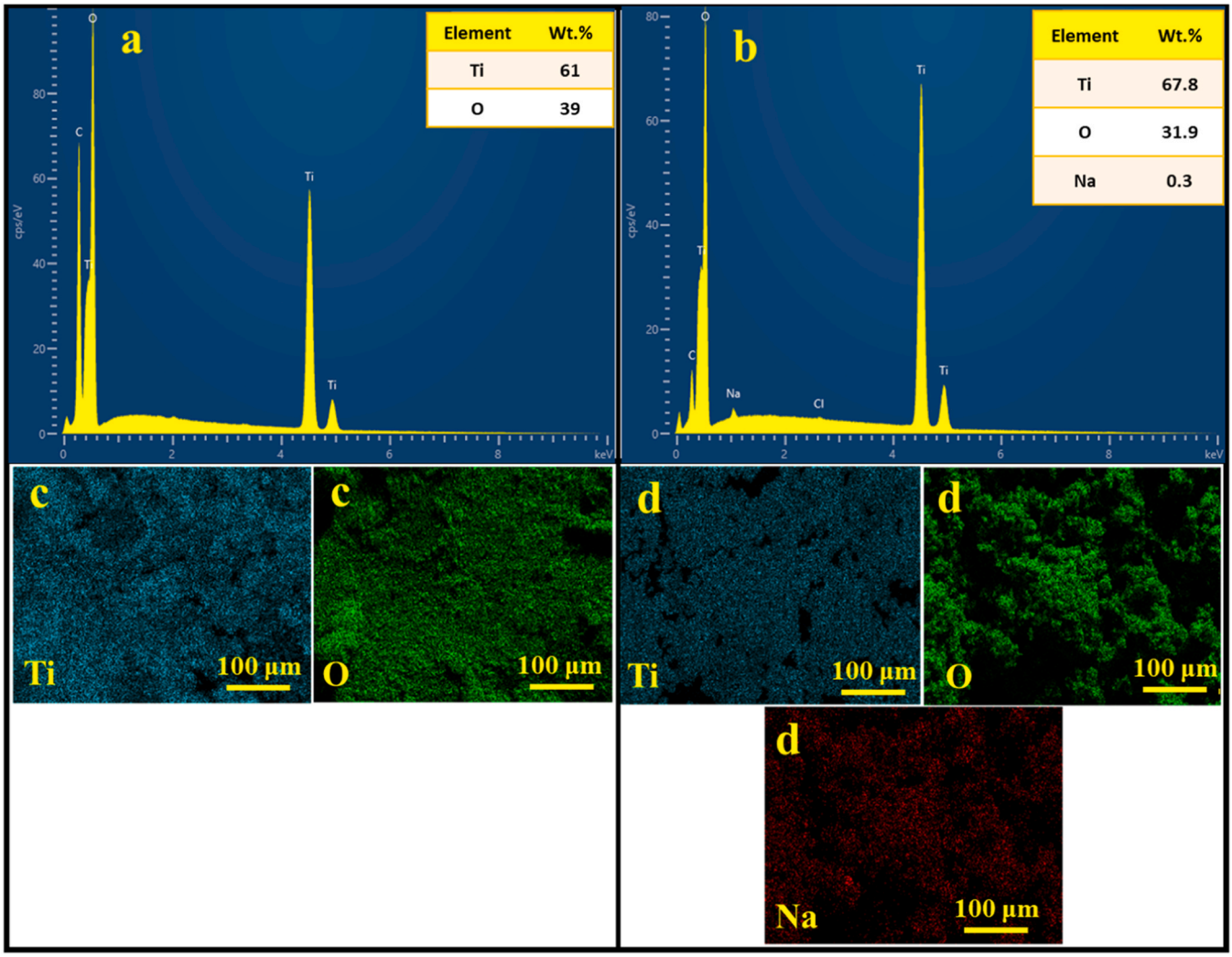

Fig. 2. EDS spectra of (a) TiO_2-NPs and (b) TiO_2-NTs; EDS mappings of (c) TiO_2-NPs and (d) TiO_2-NTs.

the as-obtained white precipitate was filtered and washed with deionized water and HCl solution (0.1 M). This process was repeated until the pH of the solution was nearly neutral. In the next step, the prepared sample underwent drying at 80 °C, and finally, the as-synthesized TiO_2-NTs were calcined at 400 °C for 2 h by a furnace (heating rate of 5 °C/min under air atmosphere).

2.2.3. *Floating TiO_2-NPs@PU and TiO_2-NTs@PU*

To prepare floating TiO_2-NPs@PU and TiO_2-NTs@PU, we coated TiO_2-NPs and TiO_2-NTs photocatalysts onto PU foam through the wet chemical deposition method. We applied porous PU foam (size: 4 cm × 1 cm, porosity: 85%) as a floating support for powder photocatalysts. To immobilize TiO_2-NPs and TiO_2-NTs onto the PU foam, we employed Polyvinyl alcohol (PVA) as a binder [29] with a weight percentage of 1 (i.e., 99 wt% photocatalysts and 1 wt% of PVA). First, PVA (1 wt%) was dissolved in deionized water (30 mL) in a three-neck flask (100 mL). The solution was heated to 95 ℃ for 3 h using a hot plate stirrer. Next, TiO_2-NPs and TiO_2-NTs photocatalysts (0.5 g) were added to the three-neck flask, followed by heating at 95 ℃ for another 2 h. The obtained solution was then transferred into a beaker (50 mL) and cooled to 80 °C. Finally, the PU foam was immersed in the aqueous suspension containing the photocatalysts and PVA and then dried in an oven at 80 °C to obtain TiO_2-NPs@PU and TiO_2-NTs@PU.

2.3. *Characterization*

We studied the wettability properties of the photocatalysts, hydrophobicity and hydrophilicity, by a Contact Angle System (OCA25, DataPhysics Instruments). The morphology and elemental compositions of the photocatalysts were investigated by a Field-Emission Scanning Electron Microscopy (FESEM, JSM-7600TFE, JEOL) equipped with Energy-Dispersive X-ray Spectroscopy (EDS). We utilized Transmission Electron Microscopy (TEM) and High-resolution Transmission Electron Microscopy (HR-TEM) to further investigate the morphology and structure of the photocatalysts (JEM-2100 F, JEOL). The size of the synthesized photocatalysts was measured by Digimizer version 5.3.5 software. The crystalline phase of the photocatalysts was characterized by an X-ray Diffractometer (XRD, D8 advance, Bruker). The crystallite size of the photocatalysts was determined by the Scherrer Equation [30].

$$D = \frac{K\lambda}{\beta\cos\theta} \tag{1}$$

In Eq. 1 , D is the crystallite size (nm), K is a constant (shape factor = 0.94), λ is the wavelength of the X-ray radiation source (Cu-Kα = 0.15406 nm), β is the full width at half maximum (FWHM) of the peak (in radian), and θ is half of the Bragg angle (in degrees).

The optical properties of the photocatalysts were examined by a Diffuse Reflectance UV–vis Spectrophotometer (DRS, Evolution™ 220, Thermo Fisher Scientific). The bandgap energy of the photocatalysts (E_g)

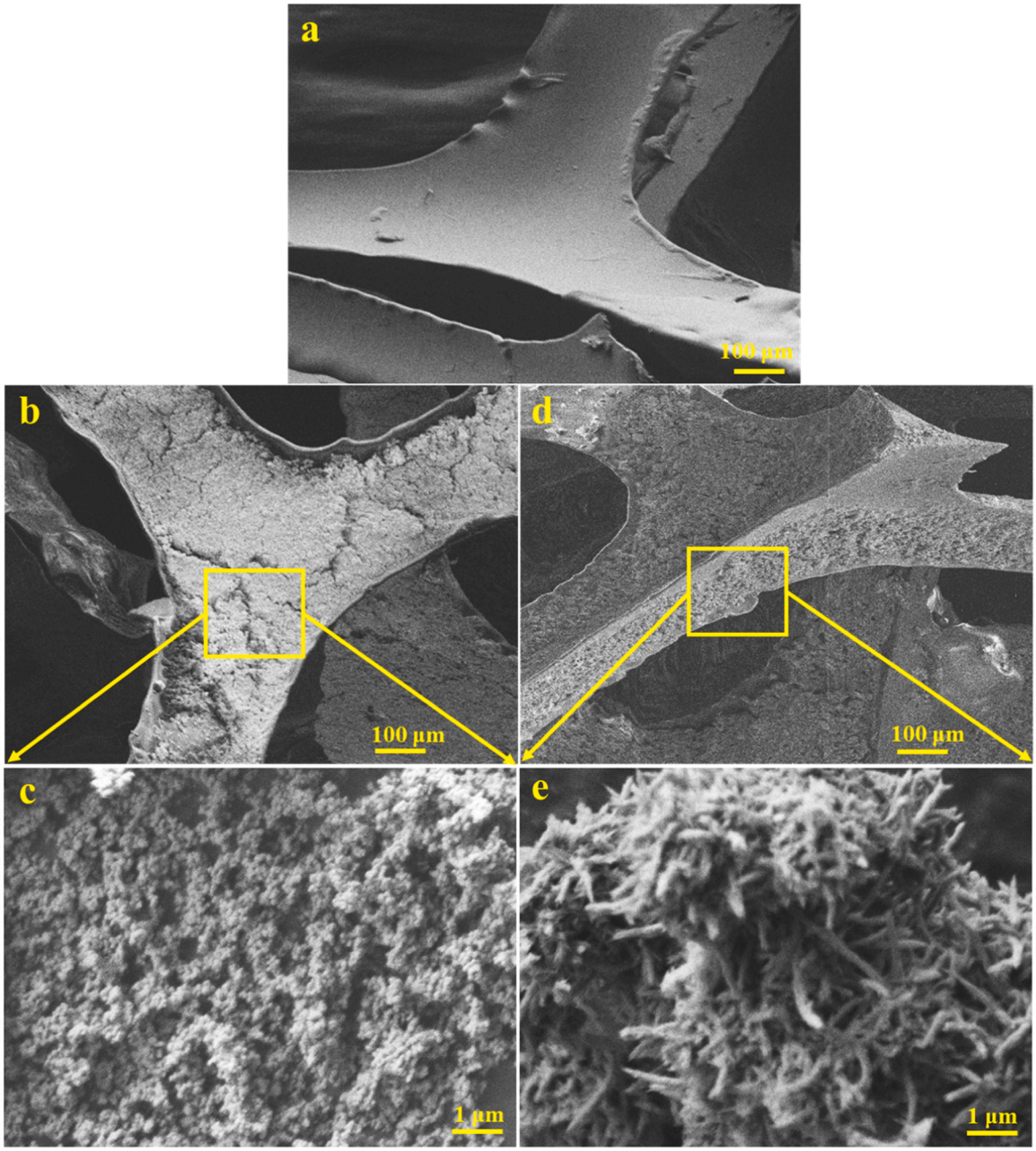

Fig. 3. SEM images of (a) pristine PU foam, (b) TiO_2-NPs@PU, (c) TiO_2-NPs, (d) TiO_2-NTs@PU, and (e) TiO_2-NTs.

was calculated by plotting $[F(R) \times h\upsilon]^{0.5}$ vs. $h\upsilon$, where F(R) is the Kubelka Munk function obtained from Eq. 2 and R is the reflectance [31, 32].

$$F(R) = \frac{(1-R)^2}{2R} \tag{2}$$

Nitrogen adsorption-desorption isotherms applying the Brunauer-Emmett-Teller method (BET) measured the specific surface area, total pore volume, and mean pore diameter of the photocatalysts by means of N_2 adsorption at 77 K (Autosorb-1 device, Quantachrome Instruments). For chemical compositions and valence states of the photocatalysts, X-ray photoelectron spectroscopy (XPS) analysis was performed by an X-ray photoelectron spectrometer microprobe (VG ESCALAB 250Xi, Thermo Scientific). Fourier Transform infrared (FTIR) spectra were performed using an FTIR Spectrometer (Thermo Scientific™, Nicolet™ iS™ 5).

2.4. Floating photocatalytic system

We evaluated the photocatalytic activity of floating TiO_2-NPs@PU and TiO_2-NTs@PU to remove BPA in a batch floating catalyst photoreactor under simulated sunlight irradiation. The experimental conditions for the removal of BPA were as follows: BPA concentration (10 mg/L), photocatalyst amount coated onto the floating PU foam (0.1 g), pH (natural, 5.7), and irradiation time (180 min). The TiO_2-NPs@PU and TiO_2-NTs@PU photocatalysts were floated in BPA solution (200 mL). The light source was a 300 W commercial solar lamp (Ultra-Vitalux, Osram) with a wavelength of 360–800 nm and an intensity of 35 W/m^2, placed 20 cm above the reactor. Before being exposed to irradiation, each sample was kept in the dark for 60 min to reach absorption-desorption equilibrium. We repeated the photocatalytic experiments three times for 180 min of simulated sunlight irradiation. Every 30 min, the BPA concentration was monitored by a UV-Vis Spectrophotometer (Evolution™ 220, Thermo Fisher Scientific) at λ_{max}= 276 nm.

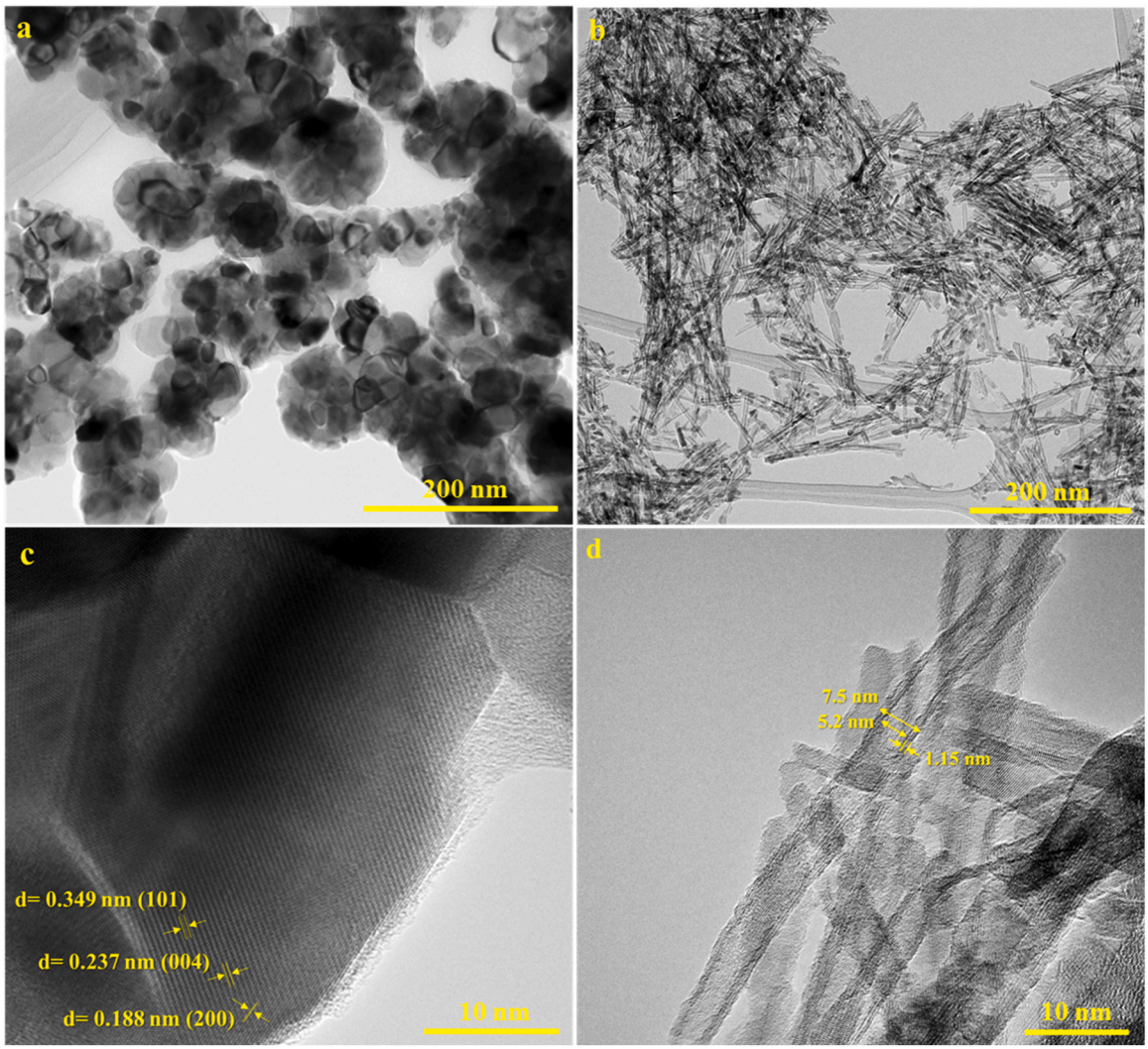

Fig. 4. TEM images of (a) TiO_2-NPs and (b) TiO_2-NTs; HR-TEM images of (c) TiO_2-NPs and (d) TiO_2-NTs.

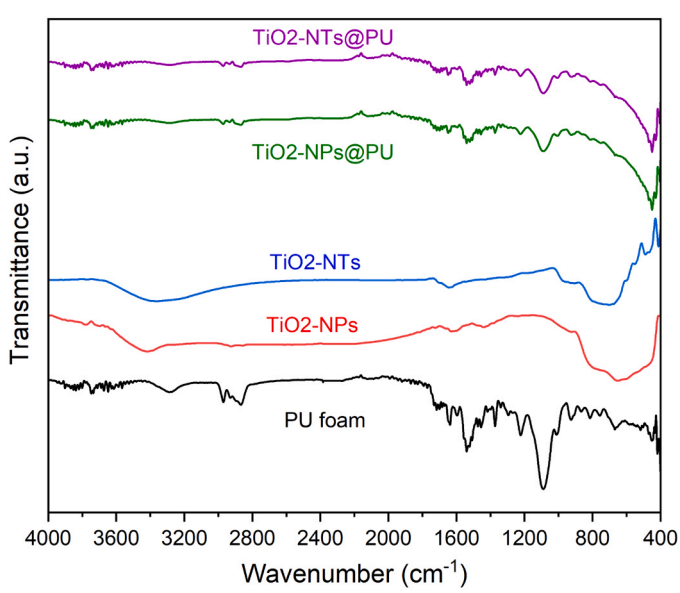

Fig. 5. FTIR spectra of PU foam, TiO_2-NPs, TiO_2-NTs, TiO_2-NPs@PU, and TiO_2-NTs@PU.

2.5. Scavenging reactive species experiments

We carried out scavenging experiments to investigate the main reactive species in removing BPA with floating TiO_2-NPs@PU and TiO_2-NTs@PU photocatalysts. We applied the following scavengers: Ammonium oxalate (AO) for photogenerated holes (h^+), Tert-butanol (t-BuOH) for hydroxyl radicals ($^{\bullet}OH$), Silver nitrate ($AgNO_3$) for electrons (e^-), and Benzoquinone (BZQ) for superoxide anions ($^{\bullet}O_2^-$). Scavenging experiments were conducted by adding 1 mM of each scavenger into the floating catalyst photoreactor under the same conditions for BPA photocatalysis experiments, as described in Section 2.4. In addition, we utilized an Electron Paramagnetic Resonance Spectrometer (EPR, Magnettech ESR5000, Bruker) with the DMPO technique to detect reactive species under simulated sunlight irradiation. Moreover, we identified intermediates during the photocatalytic degradation of BPA using High-performance Liquid Chromatography-mass Spectrometry (HPLC-MS). Samples were taken from the floating catalyst photoreactor before and after 180 min of the photocatalytic reaction.

3. Results and discussion

3.1. Wettability properties of TiO_2-NPs@PU and TiO_2-NTs@PU

Fig. 1 presents the dynamic water contact angle for pristine PU foam, TiO_2-NPs@PU, and TiO_2-NTs@PU. We examined the wettability

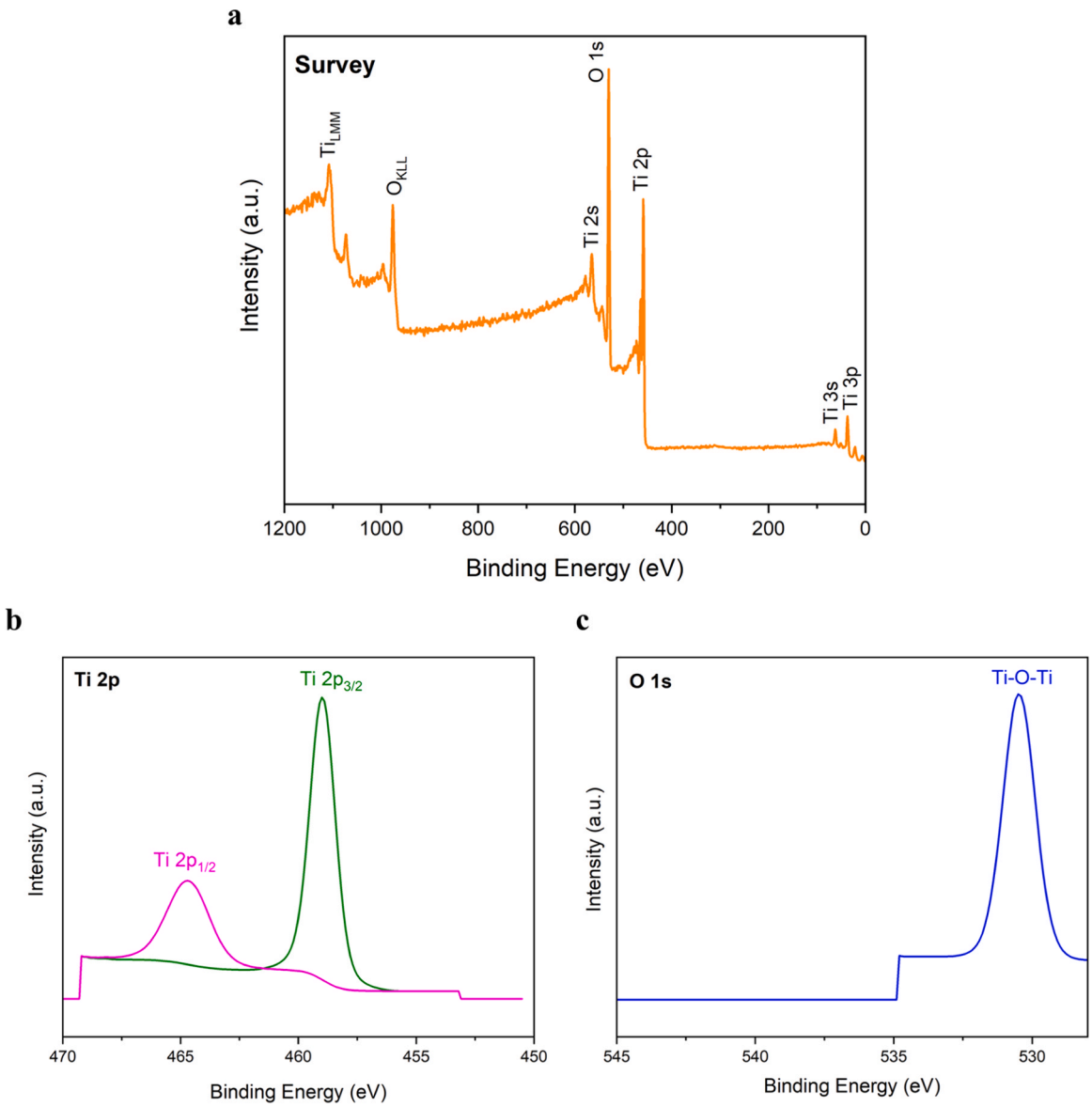

Fig. 6. XPS analysis (a) Survey spectrum of TiO_2-NTs; Spectra of (b) Ti 2p and (c) O 1 s.

properties of samples over 5 s (t≥ 5 s), with t= 0 s when the water droplet was initially formed and t= 1 s representing the time when the water droplet contacted the PU foam. As shown in Fig. 1a, the water droplet could not pass the non-coated PU foam and remained on the PU foam for over 5 s, indicating that the pristine PU foam was hydrophobic. Interestingly, introducing TiO_2-NPs on the PU foam enhanced the hydrophilicity, causing the water droplet to rapidly go through the photocatalyst and then vanish after 5 s (Fig. 1b). Consequently, floating TiO_2-NPs@PU exhibited hydrophilicity. Similarly, immobilizing TiO_2-NTs into the PU foam significantly affected hydrophilic properties. TiO_2-NTs@PU also resulted in a hydrophilic floating photocatalyst, as presented in Fig. 1c. Our findings suggest that the deposition of TiO_2 photocatalysts onto the PU foam as a floating support induced changes in the PU foam's wettability characteristics owing to the inherent hydrophilic traits of TiO_2 [33], which has potential applications in water purification.

3.2. Morphology and elemental compositions of TiO_2-NPs@PU and TiO_2-NTs@PU

EDS analysis detected the elements of Ti (61%) and O (39%) in TiO_2-NPs (Fig. 2a). Fig. 2b also indicates the presence and amount of Ti, O, and Na in TiO_2-NTs ranked in the order of 67.8%, 31.9%, and 0.3%. Moreover, the elements were uniformly dispersed in TiO_2-NPs and TiO_2-NTs, as shown in Fig. 2c and d.

Fig. 3a shows the SEM image of PU foam, indicating the smooth surface of the pristine PU foam before immobilizing TiO_2-NPs and TiO_2-NTs onto it. The SEM image of TiO_2-NPs@PU presents that TiO_2-NPs were uniformly coated into the PU foam (Fig. 3b). As depicted in Fig. 3c, the shape of the TiO_2-NPs photocatalyst synthesized by the sol-gel method was spherical. Moreover, Fig. 3d proves the successful deposition of TiO_2-NTs onto the PU foam (TiO_2-NTs@PU). Fig. 3e shows the morphology of TiO_2-NTs, confirming that the hydrothermal synthesis method successfully fabricated the nanotubular structure of TiO_2.

Fig. 4a shows the morphology of TiO_2-NPs analyzed by TEM. The TEM image indicates that the as-prepared TiO_2 photocatalyst was formed in approximately spherical nanoparticles, with an average diameter of about 32 nm measured using the Digimizer software. The internal crystalline structure of TiO_2-NPs was determined by the HR-TEM image, as depicted in Fig. 4c. The results confirmed the existence of TiO_2 anatase planes, namely (101), (004), and (200), corresponding to the d-spacing values of 0.349 nm, 0.237 nm, and 0.188 nm,

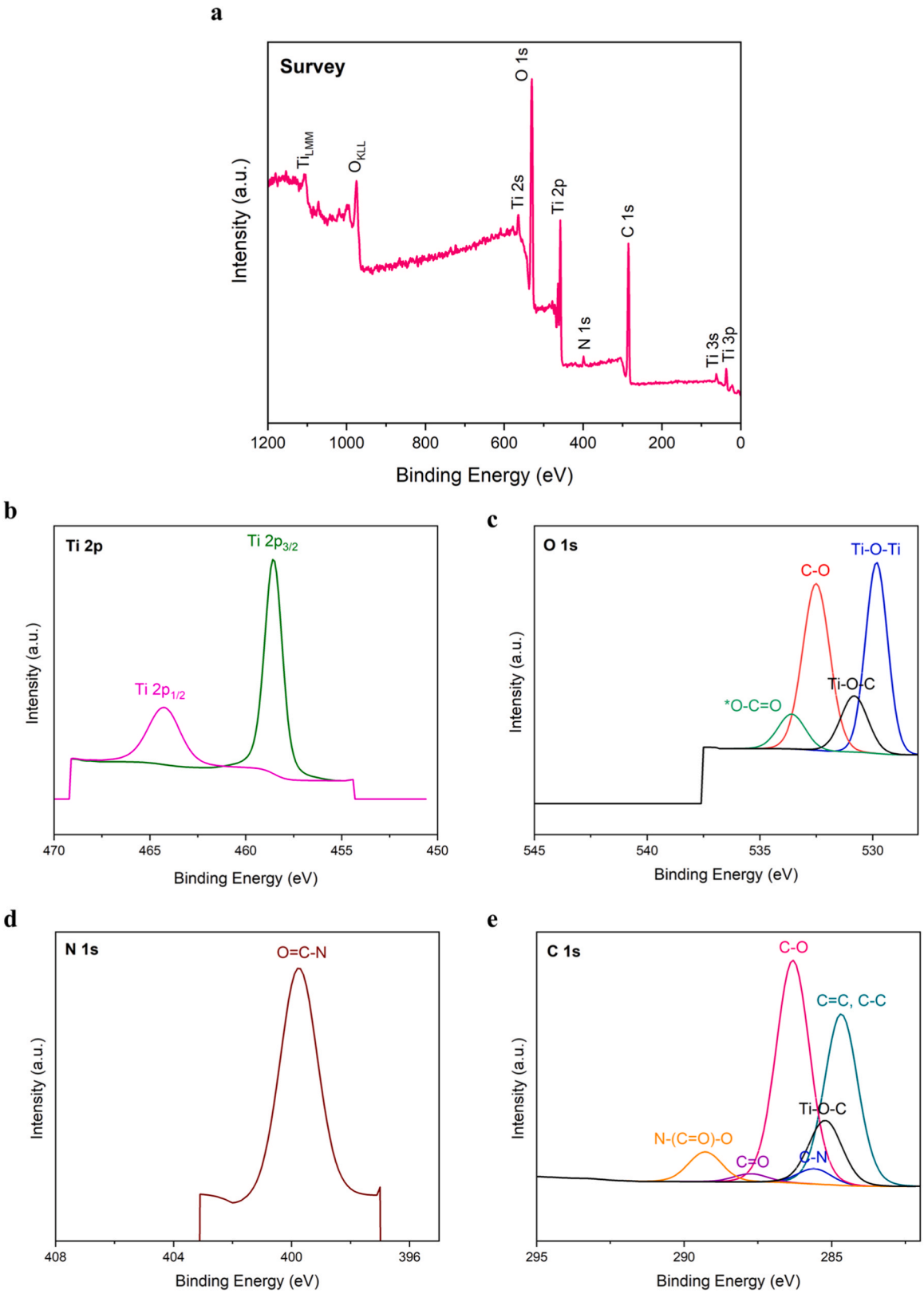

Fig. 7. XPS analysis (a) Survey spectrum of TiO_2-NTs@PU; Spectra of (b) Ti 2p, (c) O 1s, (d) N 1s, and (e) C 1s.

respectively (Reference code: 01–071–1166). In addition, Fig. 4b shows that TiO_2 photocatalysts had a hollow nanotubular structure, confirming the synthesis of TiO_2-NTs. By comparing Fig. 4b with Fig. 4a, we observed that TiO_2-NPs were transformed into TiO_2-NTs through the hydrothermal synthesis method. The transformation of TiO_2-NPs to TiO_2-NTs was reported as a sheet folding mechanism [34,35]. In the primary stage, TiO_2-NPs are dissolved, and Ti-O-Ti bonds are broken by the concentrated alkaline solution, forming Ti-O-Na and Ti-OH. In the next stage, the replacement of Na^+ and H^+ ions results in the formation and growth of layered nanosheets of sodium titanates. In the last stage,

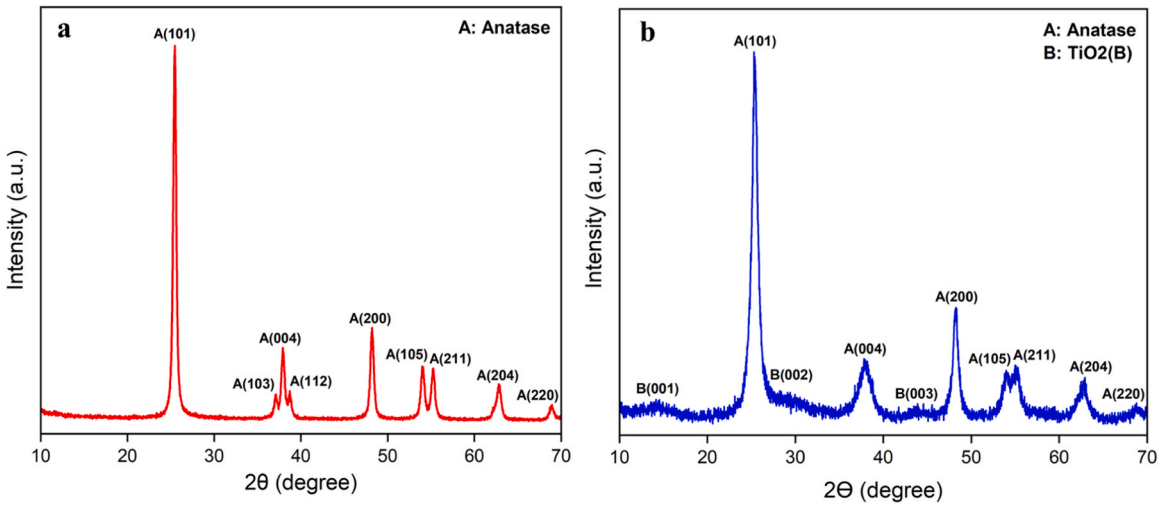

Fig. 8. XRD patterns of (a) TiO_2-NPs and (b) TiO_2-NTs.

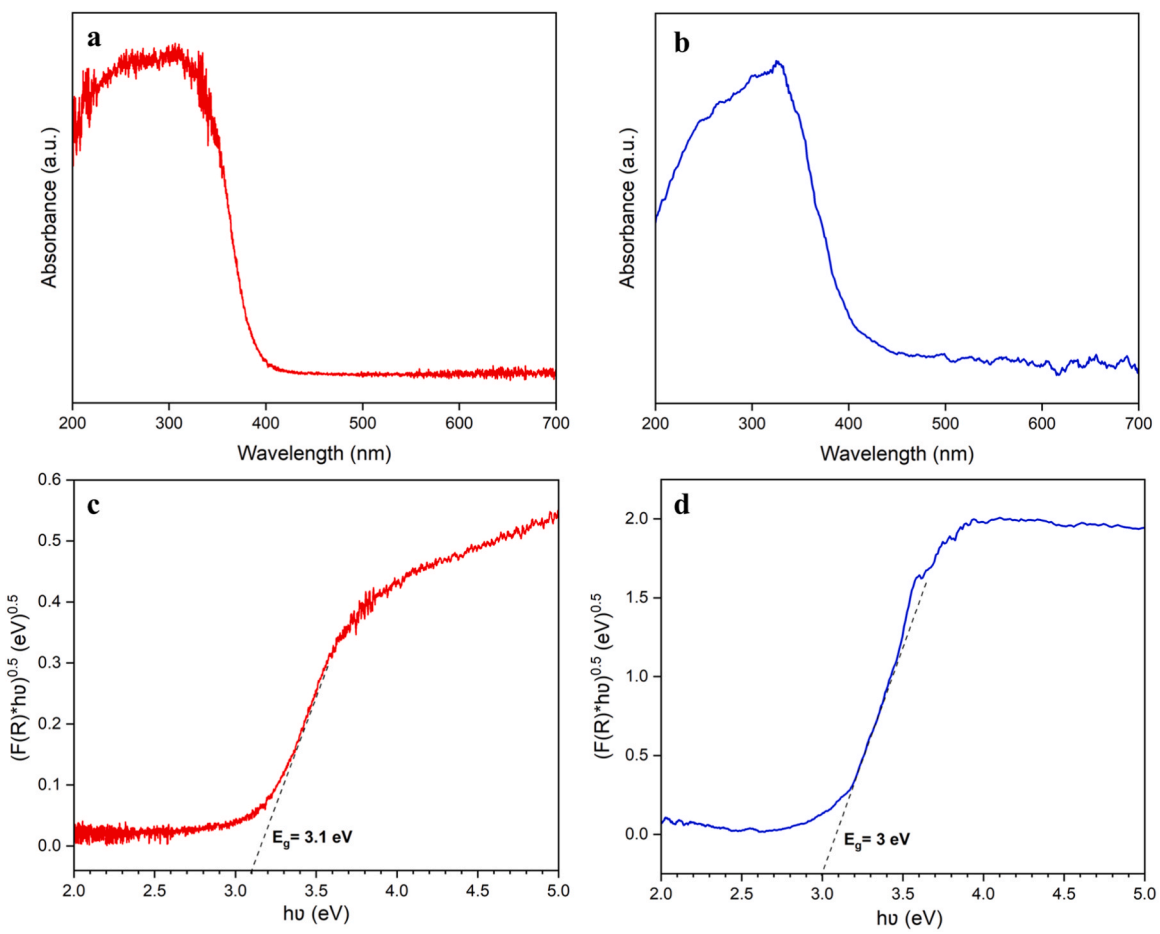

Fig. 9. DRS analysis for the absorption spectra of (a) TiO_2-NPs and (b) TiO_2-NTs; Bandgap energies of (c) TiO_2-NPs and (d) TiO_2-NTs.

the variation of surface charge caused by ion exchange of Na^+ with H^+ arising from HCl treatment causes nanosheet exfoliation and increases curling tendency, leading to the formation of nanotubes. [36]. According to the HR-TEM image of TiO_2-NTs (Fig. 4d), we measured the external diameter and internal diameter of the fabricated nanotubes, as well as the wall thickness as 7.5 nm, 5.2 nm, and 1.15 nm, respectively. Our results are consistent with previous work, including Yang et al. [37], Kubo and Nakahira [38], Hosseini and Vahabzadeh Pasikhani [28], Alkanad et al. [39], and Gilani et al. [40] who synthesized TiO_2-NTs in the same hydrothermal conditions, resulting in hollow tube-like nanostructures with an average diameter of in the range of 5–7 nm.

3.3. *Functional group detection of TiO_2-NPs@PU and TiO_2-NTs@PU*

Fig. 5 shows the FTIR spectra of PU foam, TiO_2-NPs, TiO_2-NTs, TiO_2-NPs@PU, and TiO_2-NTs@PU. In the FTIR spectrum of PU foam, the

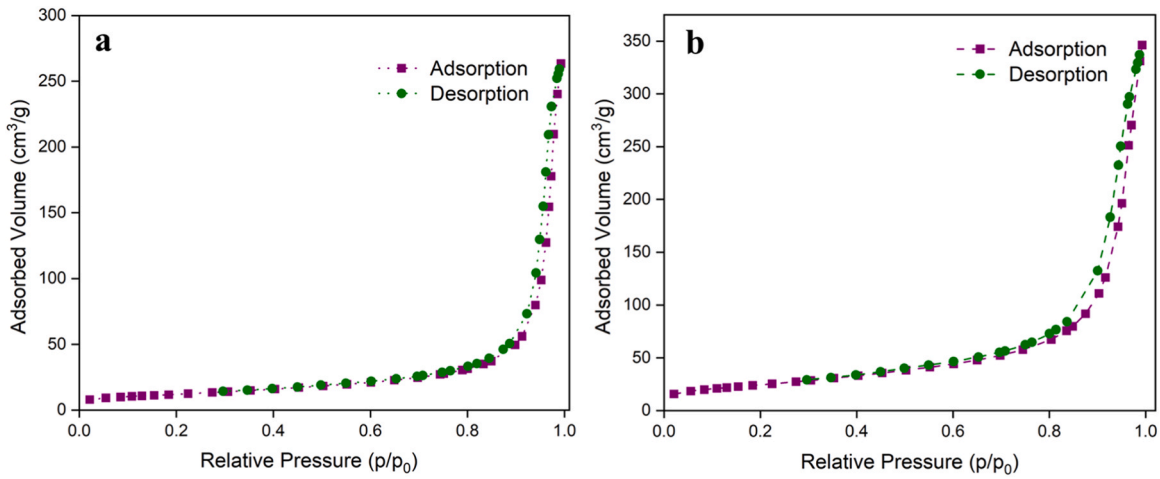

Fig. 10. N_2 adsorption-desorption isotherms of (a) TiO_2-NPs and (b) TiO_2-NTs.

Table 1
BET results of TiO_2-NPs and TiO_2-NTs.

Photocatalyst	BET Surface area (m^2/g)	Total pore volume (cm^3/g)	Mean pore diameter (nm)
TiO_2-NPs	43	0.5	37
TiO_2-NTs	89	0.6	24

peaks at around 1526 cm^{-1} and 3320 cm^{-1} were related to the in-plane bending vibration of N-H and the symmetric and asymmetric stretching vibrations of N-H, respectively. Also, the peak at near 1222 cm^{-1} indicated asymmetric stretching vibration of C-O. The vibration of C═C was identified at about 1604 cm^{-1}, and the bending vibration of C-H was observed in the range of 767–917 cm^{-1}. The peak at about 1380 cm^{-1} originated from the symmetric bending vibration of CH_3, and the peak at approximately 1083 cm^{-1} showed bond C-O-C stretch. The stretching vibrations of C-H in methyl and methylene groups were observed at about 2979 cm^{-1}, 2929 cm^{-1}, and 2873 cm^{-1} [41,42]. Regarding the FTIR spectra of TiO_2-NPs and TiO_2-NTs, the broad peaks at 700–800 cm^{-1} and 433–490 cm^{-1} corresponded to the asymmetric stretching, symmetric stretching, and the bending modes of Ti-O-Ti bonds [28]. In addition, the presence of peaks around 3420 cm^{-1} was attributed to O-H stretching of the hydroxyl group to Ti atoms (Ti-OH), and peaks observed at 1630 cm^{-1} were indexed to the stretching vibrations of H-O-H bond from water molecules adsorbed at the surface of photocatalysts [43]. As shown in Fig. 5, the FTIR spectra of TiO_2-NPs@PU and TiO_2-NTs@PU were primarily composed of the peaks of TiO_2 photocatalysts and PU foam. In addition, a shift to the high wavenumber in the FTIR spectra of TiO_2-NPs@PU and TiO_2-NTs@PU was observed owing to the hydrogen bonds formed between TiO_2 photocatalysts and PU foam [44]. Furthermore, some peaks were observed at about 790–1000 cm^{-1} in the FTIR spectra of TiO_2-NPs@PU and TiO_2-NTs@PU, which can be attributed to the vibration of Ti-O-C [28,45,46].

Table 2
Correlation coefficients and apparent rate constants for kinetics models of BPA removal.

Sample	Kinetics model					
	Correlation coefficient (R^2)			Apparent rate constant (k_{app})		
	n = 0	n = 1	n = 2	n = 0	n = 1	n = 2
TiO_2-NPs@PU	0.98	0.99	0.97	0.0226	0.0032	0.0005
TiO_2-NTs@PU	0.96	0.98	0.70	0.047	0.016	0.0115
TiO_2-NPs	0.96	0.99	0.97	0.0307	0.0045	0.0006
TiO_2-NTs	0.95	0.97	0.62	0.0615	0.0209	0.0212

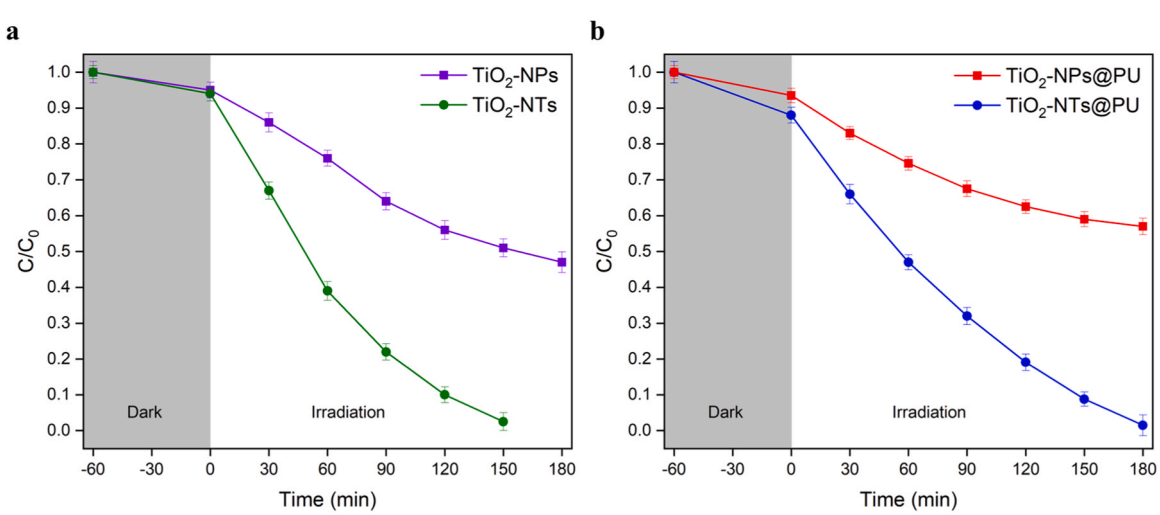

Fig. 11. BPA removal with TiO_2-NPs and TiO_2-NTs under simulated sunlight irradiation for (a) suspended and (b) floating systems.

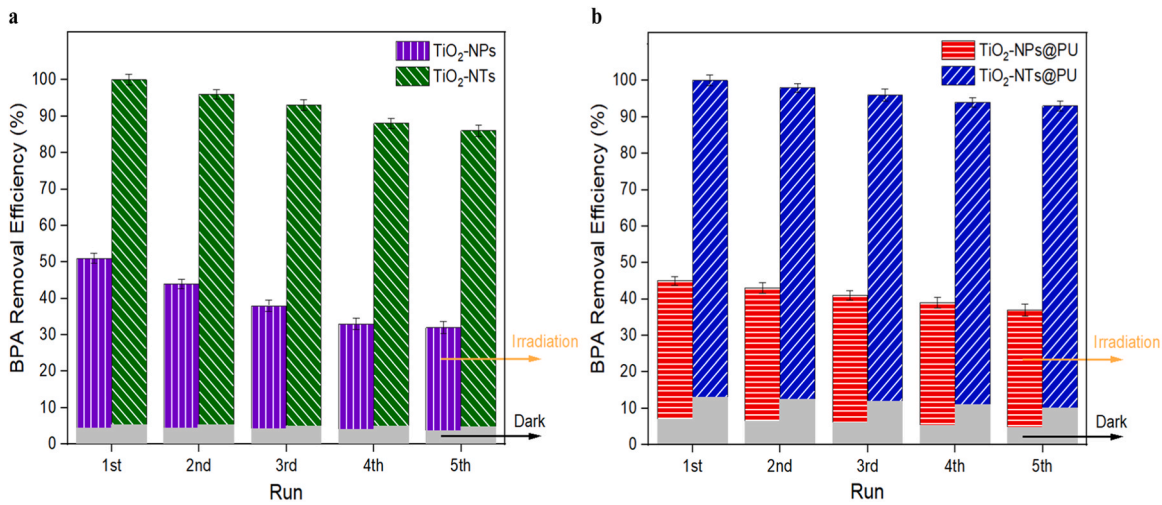

Fig. 12. Reusability of TiO_2-NPs and TiO_2-NTs for BPA removal in (a) suspended and (b) floating systems.

3.4. Chemical compositions and valence states of TiO_2-NTs and TiO_2-NTs@PU

Fig. 6a shows the XPS analysis of TiO_2-NTs, indicating the presence of Ti and O elements in the fabricated photocatalyst. Based on the high-resolution spectrum of Ti 2p (Fig. 6b), two evident peaks were observed at binding energies of 464.6 eV and 458.9 eV, which were related to Ti $2p_{1/2}$ and Ti $2p_{3/2}$ of Ti^{4+} in TiO_2, respectively [3]. In addition, Fig. 6c shows a sharp peak at a binding energy of 530.4 eV associated with the formation of lattice oxygen (Ti-O) in TiO_2 [47]. No peak related to Na was observed in XPS, implying the negligible concentration of Na in TiO_2-NTs.

Fig. 7 shows the XPS analysis of TiO_2-NTs@PU. In comparison with Fig. 6, the peaks of O 1s (530.5 eV), C 1s (284.8 eV), and N 1s (399.9 eV) were detected as characteristic of PU foam [48,49], as shown in Fig. 7a. Also, the same high-resolution spectrum was observed for Ti 2p (Fig. 7b). Regarding the spectrum of O 1s (Fig. 7c), the peak at a binding energy of 529.8 eV was related to Ti-O-Ti [48]. The peaks at 532.5 eV referred to C-O, and 533.6 eV related to O*-C═O [48,50]. In addition, the peak observed at 531.8 eV confirmed the formation of Ti-O-C [48, 51–53]. Fig. 7d shows the spectrum of N 1s, with a peak at 399.8 eV for the O═C-N group [54]. Fig. 7e shows the high-resolution spectrum of C 1 s. The peaks at 284.7 eV, 285.6 eV, 286.3 eV, 287.7 eV, and 289.3 eV were attributed to C-C, C-N, C-O, C═O, and N-(C═O)-O, respectively [48,51]. Moreover, there was a peak at 285.2 eV, referred to as Ti-O-C bonds [53].

3.5. Crystalline phase of TiO_2-NPs and TiO_2-NTs

Fig. 8 depicts the XRD pattern of TiO_2-NPs and TiO_2-NTs, indicating that TiO_2 photocatalysts exhibit a crystallized anatase structure. Fig. 8a confirmed the anatase phase of TiO_2-NPs based on the peaks at 2θ values of 25.48°, 37.04°, 37.95°, 38.67°, 48.21°, 53.92°, 55.22°, 62.84°, and 68.88° assigned to Miller indexes of (101), (103), (004), (112), (200), (105), (211), (204), and (220), respectively (JCPDS card No. 21–1272) [3,55]. Similarly, TiO_2-NTs showed the anatase phase, as confirmed by the peaks at 25.36°, 37.90°, 48.15°, 53.98°, 55.27°, and 62.86° ranked in the order of the Miller indexes of (101), (004), (200), (105), (211), (204), and (220), as shown in Fig. 8b. In addition, some peaks were observed in the XRD pattern of TiO_2-NTs at 2θ values of 15.1°, 28.6°, and 43.5°, corresponding to (001), (002), and (003) planes of TiO_2(B) phase (JCPDS No. 46–1237) [56,57]. Moreover, the crystallite size of TiO_2-NPs was 30 nm, while it was 26 nm for TiO_2-NTs, obtained by the Scherrer Equation from the anatase peak of (101). The reduction in the crystallite size of TiO_2-NTs can be justified by the hydrothermal synthesis method, which avoids the growth of TiO_2 nanocrystals [58].

3.6. Optical features of TiO_2-NPs and TiO_2-NTs

Fig. 9 reports the DRS analyses of TiO_2-NPs and TiO_2-NTs. The absorption spectra of TiO_2 nanocrystals showed an intense absorption peak in the UV region, which can be related to the electron excitation from the conduction band of TiO_2 (2p orbitals of O^{2-}) to its valence band (3d orbitals of Ti^{4+}) [59,60]. According to Fig. 9a, TiO_2-NPs had an absorption edge of about 400 nm, and the bandgap energy calculated by the Kubelka Munk function was 3.1 eV, as shown in Fig. 9c. Moreover, a redshift was observed in the absorption spectrum of TiO_2-NTs in which the absorption edge was around 415 nm (Fig. 9b), and the bandgap energy was calculated at 3 eV (Fig. 9d). The reduced bandgap energy can result from the decreased crystallite size of TiO_2-NTs (26 nm) that leads to the redshift in the absorption spectrum (Fig. 9b) and broadening of anatase peaks in the XRD pattern (Fig. 8b) [58]. Besides the crystal size, synthesizing nanotubes with an average inner diameter of 5 nm can assist in decreasing the bandgap energy to 3 eV. The same results were observed in References [61,62]. In addition, the synthesized TiO_2-NTs by alkaline hydrothermal methods led to the formation of anatase--TiO_2-B phases. Biphasic anatase-TiO_2-B phases also decreased the bandgap energy, which is reported by Peng et al. [63].

3.7. Textural properties of TiO_2-NPs and TiO_2-NTs

Fig. 10a and b show N_2 adsorption-desorption isotherms of TiO_2-NPs and TiO_2-NTs, respectively. Both TiO_2 photocatalysts presented type IV isotherms with H3 hysteresis loops based on the IUPAC classification [64]. The results indicated the slit-like mesoporous geometry of TiO_2-NPs (mean pore diameter of 37 nm) and TiO_2-NTs (mean pore diameter of 24 nm). The formation of the slit-like pore geometry by TiO_2 photocatalysts can be attributed to their aggregation, which is expected for mesoporous materials [28].

Table 1 presents BET surface area, total pore volume, and mean pore diameter of TiO_2-NPs and TiO_2-NTs. The BET surface area of TiO_2-NTs (89 m^2/g) was around two times higher than that of TiO_2-NPs (43 m^2/g). Also, as shown in Table 1, TiO_2-NTs had a total pore volume of 0.6 cm^3/g, which was greater than that of TiO_2-NPs (0.5 cm^3/g). According to the results, TiO_2-NTs fabricated by the hydrothermal method had a larger surface area than TiO_2-NPs obtained from the sol-gel method. This can be related to mesoporous walls and tube openings of TiO_2-NTs [36]. Our results are consistent with previous work. There are many studies in the literature, such as work reported by Zaki et al. [65], Rashad et al. [66], and Gilani et al. [40], which applied 160 °C to

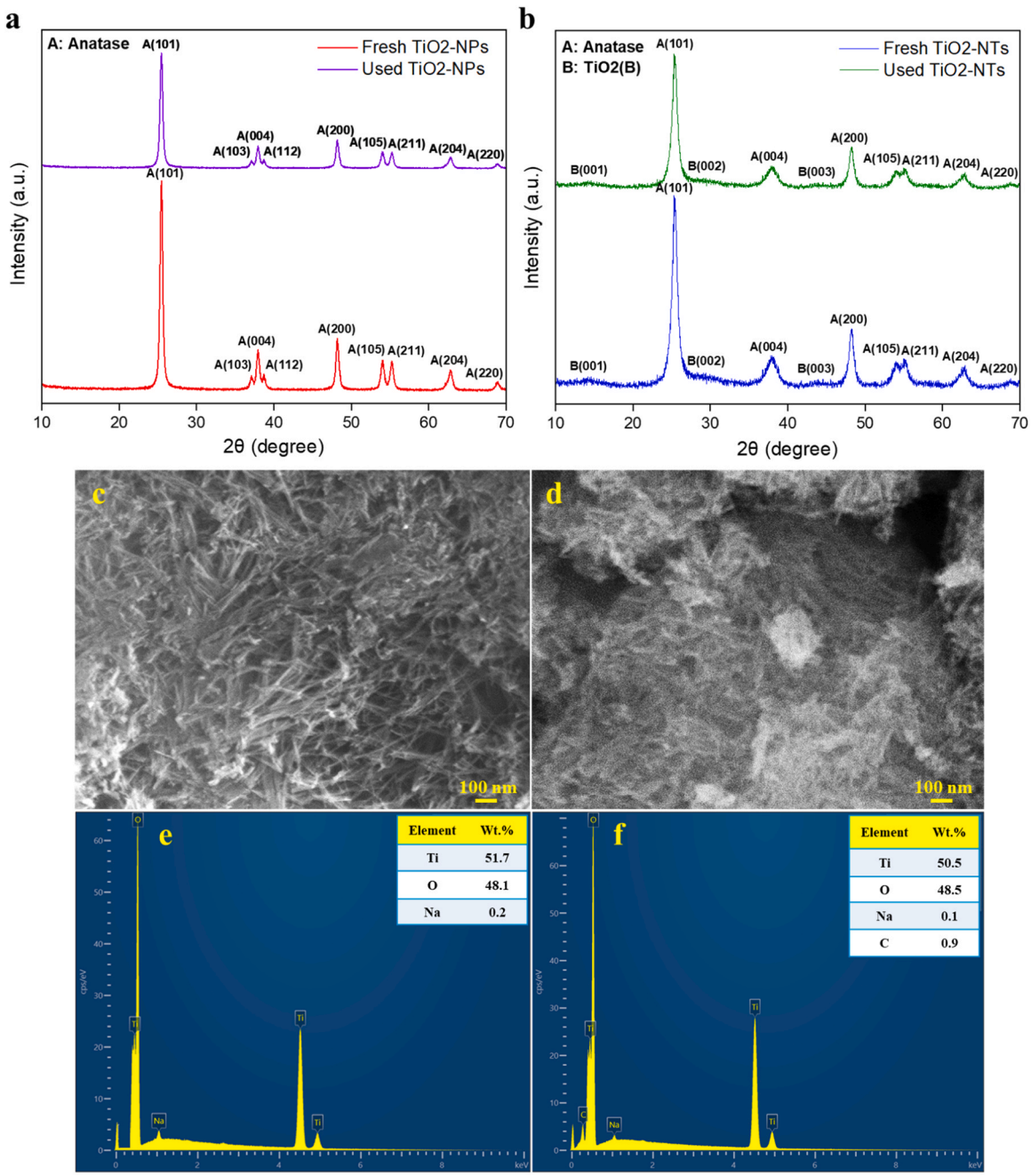

Fig. 13. XRD patterns of (a) fresh and used TiO_2-NPs@PU and (b) fresh and used TiO_2-NTs@PU; SEM images of (c) fresh TiO_2-NTs@PU and (d) used TiO_2-NTs@PU after five cycles; EDS spectra of (e) fresh TiO_2-NTs@PU and (f) used TiO_2-NTs@PU after five cycles.

prepare the anatase phase TiO_2 precursor in 10 mol/L NaOH and obtained a BET surface area in the 80–90 m^2/g range.

3.8. Photocatalytic activity of TiO_2-NPs and TiO_2-NTs for BPA removal in suspended and floating systems

Fig. 11a and b report the photocatalytic activity of TiO_2-NPs and TiO_2-NTs under simulated sunlight irradiation in suspended and floating systems, respectively. The error bars in the Figures indicate the standard deviation of replicate experiments (n=3). For all Figures, the change in BPA concentration over the first 60 min in the dark was due to the adsorption-desorption equilibrium of BPA on the surface of the photocatalysts. After the first 60 min, the light was turned on, and the change in BPA concentration correspond to the photocatalytic removal of BPA. As shown in Fig. 11a, the adsorption of BPA in the suspension system was negligible, and 4% and 6% of BPA were adsorbed on TiO_2-NPs and TiO_2-NTs, respectively. Under 180 min of simulated solar light irradiation, TiO_2-NTs had better activity than TiO_2-NPs and increased the removal of BPA from 51% to 100%. The improvement in photocatalytic activity is a consequence of engineering the optical and structural properties of TiO_2 by converting nanoparticles to 1D nanotubes [14]. As reported in Table 1, TiO_2-NTs had a surface area about two times greater than TiO_2-NPs (89 m^2/g), providing more active sites for the photocatalytic degradation of BPA. Following DRS results (Fig. 9b and d), the bandgap energy of TiO_2-NTs decreased to 3 eV, indicating improved light harvesting in the visible region, thus increasing the photocatalytic activity. Moreover, the smaller crystallite size of TiO_2-NTs (26 nm) compared to TiO_2-NPs could accelerate electron migration, resulting in

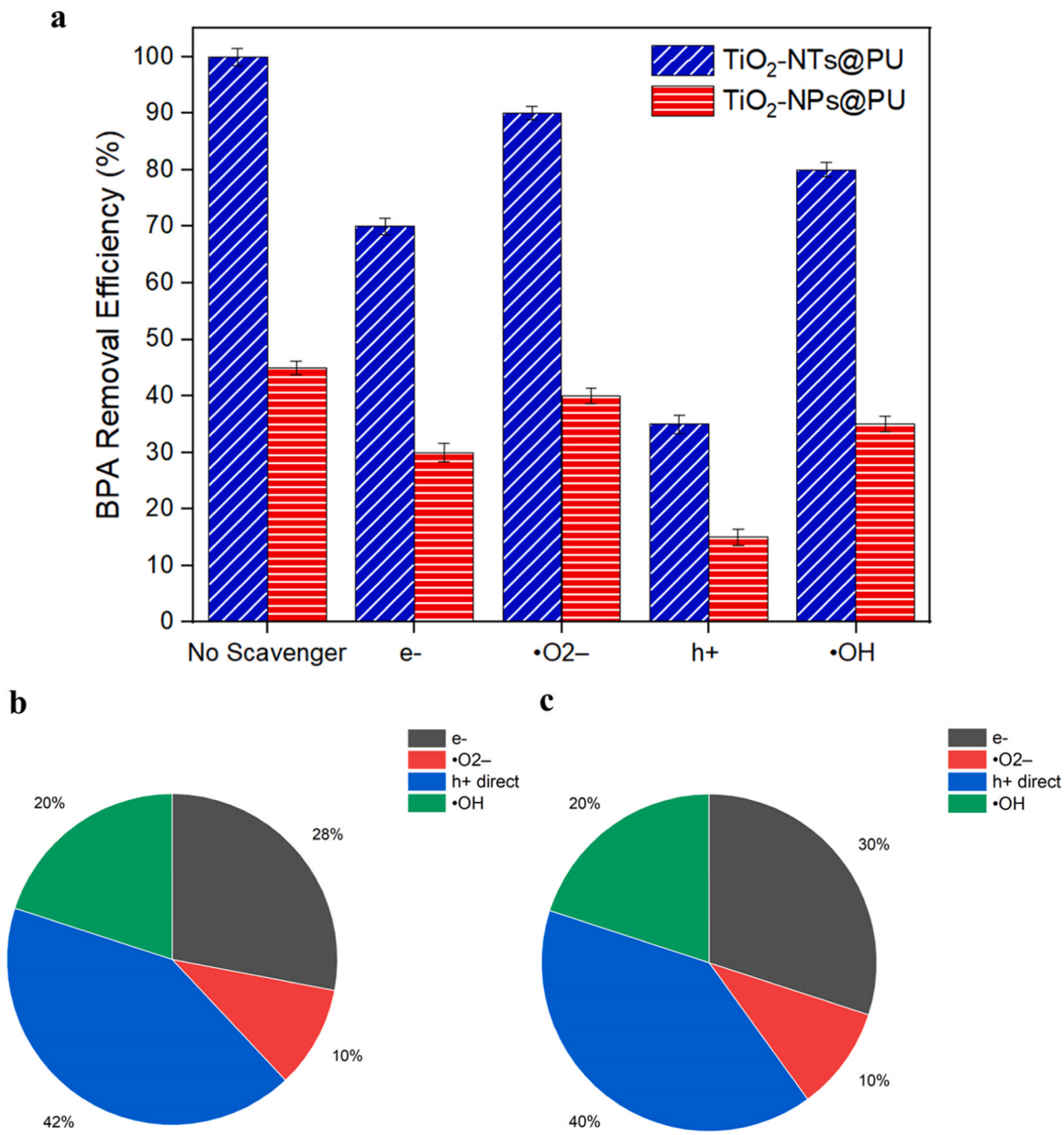

Fig. 14. (a) Free radical scavenging experiments of TiO_2-NPs@PU and TiO_2-NTs@PU for BPA removal; Reactive species contribution on BPA removal with (b) TiO_2-NTs@PU and (c) TiO_2-NPs@PU.

efficient electron-hole separation and improved BPA removal. The same trend was observed for the floating system, in which TiO_2-NTs@PU exhibited better activity than TiO_2-NPs@PU. As depicted in Fig. 11b, the BPA adsorption efficiencies over floating TiO_2-NTs@PU and TiO_2-NPs@PU were 12% and 10%, respectively. Also, the photocatalytic activity of TiO_2-NTs@PU was approximately two times higher than TiO_2-NPs@PU. BPA was completely removed by TiO_2-NTs@PU after 180 min of light irradiation, while TiO_2-NPs@PU removed only 45% of BPA under the same conditions. The results indicated that the nanotubular TiO_2 photocatalysts boosted the photocatalytic efficiency of TiO_2 for BPA removal.

The comparison between Fig. 11a and b shows that both TiO_2-NPs and TiO_2-NTs had 7% and 5% better photocatalytic activity in the suspension system than in the floating system due to the higher contact area in the suspended form [15]. Nevertheless, a floating photocatalyst is a promising system that can facilitate the recovery of photocatalysts after the process, resulting in lower operation costs and reduced runoff of materials into waters [19]. In addition, the synergistic effect of adsorption and photocatalytic degradation can contribute to the practical removal of BPA by a floating photocatalytic system. Recent studies have shown that a floating system can cause a temperature gradient at the air/water interface, which is called photothermal effect [67–69]. The photothermal effect increases oxygen absorption from the air and enhances photocatalytic reactions by increasing the concentration of reactive oxygen species in the submerged part in liquid. In addition, as shown in Fig. 11b, the photothermal effect can promote the diffusion and adsorption of BPA molecules on the floated photocatalysts' surface during the process [67].

We investigated the kinetics of BPA photocatalysis with TiO_2-NPs and TiO_2-NTs in suspended and floating systems. Eq. 3 shows the kinetics study for BPA photocatalytic removal as follows [3,59]:

$$r = -\frac{dC}{dt} = k_{app}C^n \tag{3}$$

Where k_{app} is the apparent rate constant, C is BPA concentration, t is irradiation time, and n is the photocatalytic reaction order.

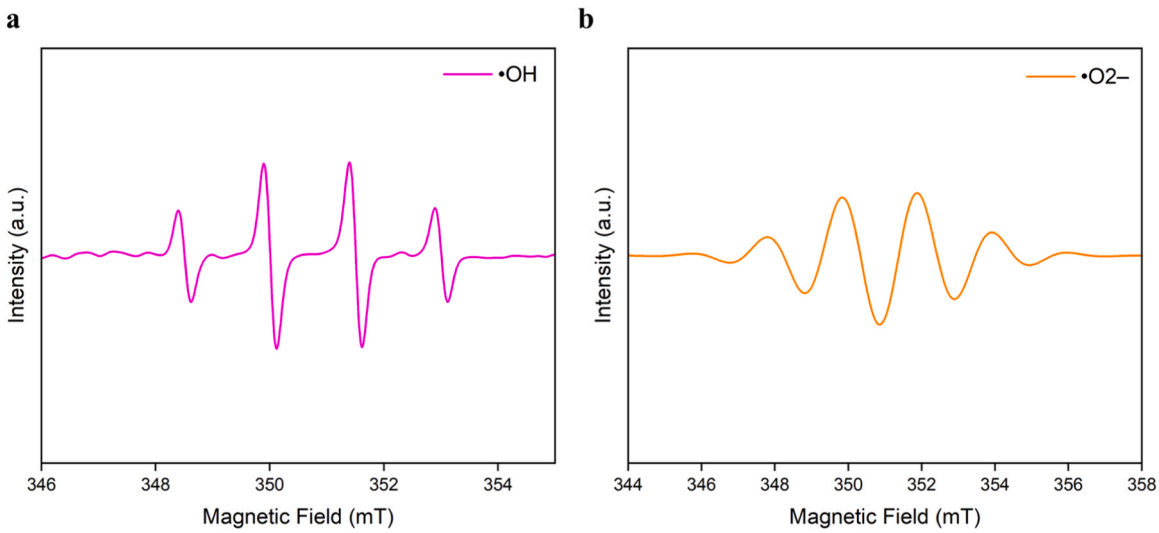

Fig. 15. ESR spectra of (a) •OH and (b) $\bullet O_2^-$ generated during BPA removal with floating TiO_2-NTs@PU under simulated sunlight irradiation.

Table 3
Identified intermediates from BPA degradation with TiO_2-NTs@PU.

Compound	*m/z*	Molecular weight
$C_{15}H_{16}O_4$	$[M+H]^+$ 261	260
$C_6H_4O_2$	$[M-H]^-$ 107	108
$C_9H_{10}O$	$[M+H]^+$ 135	134

For zero-order kinetics (n = 0), Eq. 3 can be simplified to Eq. 4.

$$C = -k_{app}t + C_0 \tag{4}$$

Moreover, Eqs. 5 and 6 present the first-order kinetics (n = 1) and the second-order kinetics (n = 2), respectively.

$$Ln\frac{C}{C_0} = -k_{app}t \tag{5}$$

$$\frac{1}{C} = k_{app}t + \frac{1}{C_0} \tag{6}$$

Where C_0 is the initial concentration of BPA.

Table 2 reports the correlation coefficients and apparent rate constants obtained based on kinetics models for BPA removal under simulated sunlight irradiation. According to Table 2, floating TiO_2-NPs@PU and TiO_2-NTs@PU photocatalysts followed the first-order kinetics ($R^2 \geq 0.98$). Also, the apparent rate constant (k_{app}) was 0.0032 min^{-1} for TiO_2-NPs@PU, and TiO_2-NTs@PU had a k_{app} of 0.016 min^{-1}. Regarding the suspended photocatalytic system, BPA photocatalysis with TiO_2-NPs and TiO_2-NTs was aligned with first-order kinetics with a k_{app} of 0.0045 min^{-1} and 0.0209 min^{-1}, respectively.

Table 4
Recent literature review on photocatalytic removal of BPA.

Photocatalyst	Pollutant	Photocatalytic system	Light and irradiation time	Removal (%)	Kinetics	Reactive species contribution	Ref.
TiO_2 P25/PU (1 g per 500 mL)	BPA 20 mg/L	Floating	UV (120 min)	71%	First order k_{app} = 0.0106 min^{-1}	h^+: NA •OH: NA e^-: NA $\bullet O_2^-$: NA	[18]
TiO_{2-x} (0.5 g/L)	BPA (10 mg/L)	Floating	Visible (60 min)	27.34%	NA	h^+: NA •OH: NA e^-: NA $\bullet O_2^-$: NA	[21]
TiO_2 nanoparticles (0.5 g/L)	BPA (10 mg/L)	Suspension	Visible light (120 min)	~20%	NA	h^+: NA •OH: NA e^-: NA $\bullet O_2^-$: NA	[74]
TiO_2 nanotubes (1 g/L)	BPA (10 mg/L)	Suspension	UV (80 min)	42%	Pseudo first order k_{app} = 0.0074 min^{-1}	h^+: NA •OH: NA e^-: NA $\bullet O_2^-$: NA	[75]
TiO_2-NPs@PU (0.1 g per 200 mL)	BPA (10 mg/L)	Floating	Simulated sunlight (180 min)	45%	First order k_{app} = 0.0032 min^{-1}	h^+: 40% •OH: 20% e^-: 30% $\bullet O_2^-$: 10%	Present work
TiO_2-NTs@PU (0.1 g per 200 mL)	BPA (10 mg/L)	Floating	Simulated sunlight (180 min)	100%	First order k_{app} = 0.016 min^{-1}	h^+: 42% •OH: 20% e^-: 28% $\bullet O_2^-$: 10%	Present work

3.9. Reusability of TiO_2-NPs and TiO_2-NTs for BPA removal in suspended and floating systems

According to Fig. 12a, the photocatalytic activity of suspended TiO_2-NPs and TiO_2-NTs decreased from 51% to 32% and from 100% to 86% after five cycles, mainly due to the photocatalyst loss and poisoning of active sites with degraded products [59,70]. As shown in Fig. 12b, the BPA removal by floating TiO_2-NTs@PU declined to 93% after five cycles, which can be due to the poisoning of active sites in the photocatalyst with degraded products [59]. Regarding floating TiO_2-NPs@PU, the photocatalyst maintained its activity after five recycling steps, with an 8% decrease in BPA removal efficiency. Floating photocatalysts can be reused several consecutive times without significant decrease in photocatalytic activity as opposed to the suspension system [20].

We investigated the structure and morphology of floating TiO_2-NPs@PU and TiO_2-NTs@PU photocatalysts after five reuse cycles. Fig. 13a and b show no change in the XRD patterns of fresh and used photocatalysts. Thus, the results confirmed the structural stability of TiO_2-NPs@PU and TiO_2-NTs@PU after five cycles. In addition, Fig. 13c and d show that the nanotubular structure of TiO_2-NTs did not change after five cycles, implying its stability. Only a few particles appeared on the surface of TiO_2-NTs, which corresponds to the poisoning of active sites with degraded products based on EDS results (i.e., the presence of C elements after the process), which can explain the decline in the photocatalytic activity.

3.10. Mechanism of BPA removal by floating TiO_2-NPs@PU and TiO_2-NTs@PU

Fig. 14a shows the results of free radical scavenging of h^+, $^{\bullet}OH$, e^-, and $^{\bullet}O_2^-$ generated during BPA photocatalysis with TiO_2-NPs@PU and TiO_2-NTs@PU under simulated sunlight irradiation. Regarding TiO_2-NTs@PU, adding ammonium oxalate (AO) as h^+ scavengers to the floating photocatalytic system significantly decreased BPA removal from 100% to 35%. This indicates that h^+ was the main reactive species in the BPA photocatalysis compared to other scavengers. Besides, we determined the contribution of each reactive species (h^+, $^{\bullet}OH$, e^-, and $^{\bullet}O_2^-$) affecting BPA removal over TiO_2-NTs@PU and TiO_2-NPs@PU, as it is shown in Figs. 14b and 14c, respectively. According to Fig. 14b, the contribution of h^+ (direct) in the photocatalytic removal of BPA with TiO_2-NTs@PU was 42%. Also, $^{\bullet}OH$, e^-, and $^{\bullet}O_2^-$ were the other reactive species, which accounted for 20%, 28%, and 10% of the BPA removal, respectively. Moreover, Fig. 14c presents the same trend for TiO_2-NPs@PU in the photocatalytic removal of BPA. As it is shown in Fig. 14c, the dominant free radical scavenging in BPA photocatalysis with TiO_2-NPs@PU was h^+ (direct), with a contribution of 40%. In addition, $^{\bullet}OH$, e^-, and $^{\bullet}O_2^-$ had a 20%, 30%, and 10% contribution to the BPA removal, respectively.

Further, Fig. 15 shows that signals detected in the ESR, confirming the generation of $\bullet OH$ and $\bullet O_2^-$ [71] during the removal of BPA with floating TiO_2-NTs@PU under simulated sunlight irradiation.

Table 3 shows intermediates generated during the photodegradation of BPA with floating TiO_2-NTs@PU via HPLC-MS analysis. According to the detected intermediates, BPA photocatalytic degradation occurred based on oxidation and β-scission reactions [72]. The detected intermediate $C_{15}H_{16}O_4$ ($m/z = 261$) was a result of BPA oxidation [72]. The formation of $C_9H_{10}O$ ($m/z = 135$) and $C_6H_4O_2$ ($m/z = 107$) arose from the β-scission of BPA [73]. Further progress of the reaction can lead to the mineralization of these intermediates, producing CO_2 and H_2O [72, 73]. These results confirm that TiO_2-NTs@PU was able to degrade BPA under simulated sunlight irradiation.

3.11. Comparison of floating TiO_2-NTs@PU with previous work

Table 4 shows the recent literature review on the photocatalytic removal of BPA. Only two works have been reported to remove BPA using floating photocatalytic systems. Li et al. [18] fabricated floating photocatalysts based on a PU foam with P25 nanoparticles, the commercial TiO_2 benchmark, to remove BPA. The removal of BPA was 71% after 120 min of UV irradiation based on a first-order kinetics. In another study [21], about 27% of BPA was removed by floating TiO_{2-x} under visible light after 60 min irradiation. The literature seems to lack kinetic studies on BPA removal with floating TiO_{2-x}. Further, the contribution of reactive species in the photocatalytic removal of BPA has not been investigated [18,21]. Krishnan et al. [74] synthesized TiO_2 nanoparticles for BPA removal in a suspended system, resulting in about 20% degradation under visible light (120 min). Also, the synthesized TiO_2 nanotubes by Doong and Tsai [75] reached 42% of BPA removal under UV irradiation for 80 min. In this work, for the first time, we investigated the effect of the TiO_2 nanotubular structure on the activity of floating photocatalytic systems for BPA removal under simulated sunlight. In addition, we compared the photocatalytic activity of floating systems with that of suspended ones. The BPA removal efficiency was 45% for floating TiO_2-NPs@PU, while it was 100% for floating TiO_2-NTs@PU after 180 min of simulated sunlight irradiation. Moreover, we examined the mechanism of BPA degradation with floating photocatalysts by determining reactive species contribution, which other researchers have not reported. Finally, floating TiO_2-NTs@PU photocatalysts constitute a promising approach to removing contaminants from water.

4. Conclusions

We synthesized floating TiO_2-NPs@PU photocatalysts by the sol-gel method and TiO_2-NTs@PU by the ultrasound-assisted hydrothermal method, followed by wet chemical deposition. The results confirmed the successful anchoring of TiO_2-NPs and TiO_2-NTs onto the porous PU foam, resulting in hydrophilic floating photocatalysts. Morphological characterizations indicated that the hydrothermal synthesis method successfully fabricated the nanotubular TiO_2 photocatalysts. The photocatalysts were crystalline TiO_2 anatase with a crystallite size of 26 nm for TiO_2-NTs. DRS results showed a reduced bandgap energy of 3 eV for TiO_2-NTs. The nanotubular structure of TiO_2 photocatalysts prepared by the hydrothermal method increased the surface area to 89.6 m^2/g. According to the results, 0.1 g of TiO_2-NTs@PU eliminated 10 mg/L of BPA after 180 min of exposure to simulated sunlight (300 W commercial solar lamp and intensity of 35 W/m^2), while the photocatalytic removal of BPA was 45% with TiO_2-NPs@PU. The fabricated photocatalysts remained stable after five consecutive cycles. In addition, the dominant free radical scavenging during BPA photocatalysis was identified as h^+.

CRediT authorship contribution statement

Daria Camilla Boffito: Data curation, Funding acquisition, Investigation, Methodology, Project administration, Resources, Supervision, Writing – review & editing. **Claudia L. Bianchi:** Data curation, Funding acquisition, Investigation, Methodology, Project administration, Writing – review & editing. **Viviane Yargeau:** Data curation, Investigation, Methodology, Project administration, Supervision, Writing – review & editing. **Nila Davari:** Conceptualization, Data curation, Formal analysis, Investigation, Methodology, Validation, Visualization, Writing – original draft. **Ermelinda Falletta:** Data curation, Investigation, Methodology, Writing – review & editing.

Declaration of Competing Interest

The authors declare that they have no known competing financial interests or personal relationships that could have appeared to influence the work reported in this paper.

Data availability

Data will be made available on request.

Acknowledgments

The authors thank Velux Stiftung Foundation for the financial support through the project 1381 “SUNFLOAT - Water decontamination by sunlight-driven floating photocatalytic systems”. We also appreciate the support of Bourse d’excellence Neil R. Mitchell et Danièle Dumais (Quebec, Canada).

References

[1] Y. Wei, Q. Wu, H. Meng, Y. Zhang, C. Cao, Recent advances in photocatalytic self-cleaning performances of TiO2-based building materials, RSC Adv. 13 (2023) 20584–20597.
[2] A. Tabet, L. Zougar, M. Djebbouri, S. Sali, S. Kermadi, O. Mahroua, A. Mahieddine, M. Trari, Photo-electrochemical properties of nanostructured metal-semiconductorAl/TiO2 thin film. Application to Rhodamine B oxidation under sunlight, Optik 249 (2022) 168288.
[3] M. Riyaheini, N. Gilani, J.V. Pasikhani, Engineering the photo-induced charge generation between TiO2 and FeS2 heterojunction for enhanced photocatalytic wastewater purification, Ceram. Int. (2023).
[4] Q. Kang, S. Ning, D. Jiang, Y. Wang, F. Zhou, Chapter 16 - Semiconductor-based artificial photosynthesis for water-splitting and CO2 reduction, in: H.J.M. Hou, S. I. Allakhverdiev (Eds.), Photosynthesis, Academic Press, 2023, pp. 377–405.
[5] Z. Huang, H. Liu, Insights into the pathways, intermediates, influence factors and toxicological properties in the degradation of tetracycline by TiO2-based photocatalysts, J. Environ. Chem. Eng. 11 (2023) 110587.
[6] S.N. Sadikin, J. Ridwan, M.I.A. Umar, A.A.M. Raub, J. Yunas, A.A. Hamzah, D. Dahlan, M.Y.A. Rahman, A.A. Umar, Photocatalytic activity and stability properties of porous TiO2 film as photocatalyst for methylene blue and methylene orange degradation, Int. J. Electrochem. Sci. 18 (2023) 100246.
[7] D. Beketova, M. Motola, H. Sopha, J. Michalicka, V. Cicmancova, F. Dvorak, L. Hromadko, B. Frumarova, M. Stoica, J.M. Macak, One-step decoration of TiO2 nanotubes with Fe3O4 nanoparticles: synthesis and photocatalytic and magnetic properties, ACS Appl. Nano Mater. 3 (2020) 1553–1563.
[8] N.K. Shrestha, J.M. Macak, F. Schmidt-Stein, R. Hahn, C.T. Mierke, B. Fabry, P. SchmukiMagnetically guided titania nanotubes for site-selective photocatalysis and drug release, 48, 2009. pp. 969-972..
[9] D. Kanakaraju, F.D. anak Kutiang, Y.C. Lim, P.S. Goh, Recent progress of Ag/TiO2 photocatalyst for wastewater treatment: doping, co-doping, and green materials functionalization, Appl. Mater. Today 27 (2022) 101500.
[10] T.M. Pham, K.Q. Bui, D.V. Le, H.Q. Pham, T.T. Huynh, T.M. Ngo, V.T.T. HoVisible light-driven N–F-codoped TiO2 for photocatalysts as potential application to wastewater treatment, 46, 2023. pp. 865-872..
[11] H.-Y. Yang, W.-Y. Rho, S.K. Lee, S.H. Kim, Y.-B. HahnTiO2 nanoparticles/nanotubes for efficient light harvesting in perovskite solar cells, 9, 2019. p. 326..
[12] H.H. Nguyen, G. Gyawali, A. Martinez-Oviedo, Y.K. Kshetri, S.W. Lee, Physicochemical properties of Cr-doped TiO2 nanotubes and their application in dye-sensitized solar cells, J. Photochem. Photobiol. A: Chem. 397 (2020) 112514.
[13] A. Bjelajac, R. Petrović, V. Djokic, V. Matolin, M. Vondraček, K. Dembele, S. Moldovan, O. Ersen, G. Socol, I.N. Mihailescu, D. Janaćković, Enhanced absorption of TiO2 nanotubes by N-doping and CdS quantum dots sensitization: insight into the structure, RSC Adv. 8 (2018) 35073–35082.
[14] J.M. Macak, M. Zlamal, J. Krysa, P. SchmukiSelf-organized TiO2 nanotube layers as highly efficient photocatalysts, 3, 2007. pp. 300-304..
[15] M. Zlamal, J.M. Macak, P. Schmuki, J. Krýsa, Electrochemically assisted photocatalysis on self-organized TiO2 nanotubes, Electrochem. Commun. 9 (2007) 2822–2826.
[16] O. Zakir, A. Ait-Karra, R. Idouhli, M. Khadiri, B. Dikici, A. Aityoub, A. Abouelfida, A. Outzourhit, A review on TiO2 nanotubes: synthesis strategies, modifications, and applications, J. Solid State Electrochem. 27 (2023) 2289–2307.
[17] N. Liu, X. Chen, J. Zhang, J.W. Schwank, A review on TiO2-based nanotubes synthesized via hydrothermal method: formation mechanism, structure modification, and photocatalytic applications, Catal. Today 225 (2014) 34–51.
[18] L. Li, Y. Li, H. Xu, W. Zhang, Novel floating TiO2 photocatalysts for polluted water decontamination based on polyurethane composite foam, Sep. Sci. Technol. 50 (2015) 164–173.
[19] N.H. Mohamad Idris, K.Y. Cheong, S.M. Smith, H.L. Lee, C,N-Codoped TiO2 nanoparticles immobilized on floating alginate beads for diazinon removal under solar light irradiation, ACS Appl. Nano Mater. (2023).
[20] C.T. Mehmood, Z. Zhong, H. Zhou, C. Zhang, Y. Xiao, Immobilizing a visible light-responsive photocatalyst on a recyclable polymeric composite for floating and suspended applications in water treatment, RSC Adv. 10 (2020) 36349–36362.
[21] Y. Cai, Y. Chen, S. Ge, X. Qu, N. Sheng, L. Yang, S. Chen, H. Wang, A. Hagfeldt, Co-doped magnetic N-TiO2-x/rGO heterojunction@cellulose nanofibrous flakelet for enhanced photocatalytic oxidation and facile separation: efficient charge separation and self-floatability, Chem. Eng. J. 425 (2021) 131462.
[22] Z. Xing, J. Zhang, J. Cui, J. Yin, T. Zhao, J. Kuang, Z. Xiu, N. Wan, W. Zhou, Recent advances in floating TiO2-based photocatalysts for environmental application, Appl. Catal. B: Environ. 225 (2018) 452–467.
[23] L. Ni, Y. Li, C. Zhang, L. Li, W. Zhang, D. Wang, Novel floating photocatalysts based on polyurethane composite foams modified with silver/titanium dioxide/graphene ternary nanoparticles for the visible-light-mediated remediation of diesel-polluted surface water, 133 (2016).
[24] L. Zhang, Z. Xing, H. Zhang, Z. Li, X. Zhang, Y. Zhang, L. Li, W. ZhouMultifunctional floating titania-coated macro/mesoporous photocatalyst for efficient contaminant removal, 80, 2015. pp. 623-629..
[25] L.S. Mendieta-Rodríguez, L.M. González-Rodríguez, J.J. Alcaraz-Espinoza, A. E. Chávez-Guajardo, J.C. Medina-Llamas, Synthesis and characterization of a polyurethane-polyaniline macroporous foam material for methyl orange removal in aqueous media, Mater. Today Commun. 26 (2021) 102155.
[26] L. Zhang, Z. Xing, H. Zhang, Z. Li, X. Wu, X. Zhang, Y. Zhang, W. Zhou, High thermostable ordered mesoporous SiO2–TiO2 coated circulating-bed biofilm reactor for unpredictable photocatalytic and biocatalytic performance, Appl. Catal. B: Environ. 180 (2016) 521–529.
[27] Z. Khani, D. Schieppati, C.L. Bianchi, D.C. BoffitoThe sonophotocatalytic degradation of pharmaceuticals in water by MnOx-TiO2 systems with tuned band-gaps, 9, 2019. p. 949..
[28] S.G. Hosseini, J.V. Pasikhani, Enhanced optical properties and photocatalytic activity of TiO2 nanotubes by using magnetic activated carbon: evaluating photocatalytic reduction of Cr(VI), Environ. Technol. 42 (2021) 914–931.
[29] H. Taghvaei, E. Pirzadeh, M. Jahanbakhsh, O. Khalifeh, M.R. Rahimpour, Polyurethane foam: a novel support for metal oxide packing used in the non-thermal plasma decomposition of CO2, J. CO2 Util. 44 (2021) 101398.
[30] S. Aflaki, M. Farhadian, A.R. Solaimany Nazar, S. Tangestaninejad, N. Davari, Investigation of copper plates as anode and TiO2/glycine/ZnFe2O4 stabilized on graphite as cathode for textile dyes degradation from aqueous solution under visible light, J. Appl. Electrochem. 51 (2021) 1387–1405.
[31] N. Davari, M. Farhadian, A.R.S. Nazar, M. Homayoonfal, Degradation of diphenhydramine by the photocatalysts of ZnO/Fe2O3 and TiO2/Fe2O3 based on clinoptilolite: structural and operational comparison, J. Environ. Chem. Eng. 5 (2017) 5707–5720.
[32] N. Davari, M. Farhadian, A.R. Solaimany, Nazar, Synthesis and characterization of Fe2O3 doped ZnO supported on clinoptilolite for photocatalytic degradation of metronidazole, Environ. Technol. 42 (2021) 1734–1746.
[33] Y. Kameya, H. YabeOptical and superhydrophilic characteristics of TiO2 coating with subwavelength surface structure consisting of spherical nanoparticle aggregates, 9, 2019. p. 547..
[34] Y.Q. Wang, G.Q. Hu, X.F. Duan, H.L. Sun, Q.K. Xue, Microstructure and formation mechanism of titanium dioxide nanotubes, Chem. Phys. Lett. 365 (2002) 427–431.
[35] X. Sun, Y. LiSynthesis and characterization of ion-exchangeable titanate nanotubes, 9, 2003. pp. 2229-2238..
[36] L. Niu, X. Zhao, Z. Tang, H. Lv, F. Wu, X. Wang, T. Zhao, J. Wang, A. Wu, J. P. Giesy, Difference in performance and mechanism for methylene blue when TiO2 nanoparticles are converted to nanotubes, J. Clean. Prod. 297 (2021) 126498.
[37] J. Yang, J. Du, X. Li, Y. Liu, C. Jiang, W. Qi, K. Zhang, C. Gong, R. Li, M. Luo, H. PengHighly hydrophilic TiO2 nanotubes network by alkaline hydrothermal method for photocatalysis degradation of methyl orange, 9, 2019. p. 526..
[38] T. Kubo, A. Nakahira, Local structure of TiO2-derived nanotubes prepared by the hydrothermal process, J. Phys. Chem. C 112 (2008) 1658–1662.
[39] K. Alkanad, A. Hezam, N. Al-Zaqri, M.A. Bajiri, G. Alnaggar, Q.A. Drmosh, H. A. Almukhlifi, L. Neratur Krishnappagowda, One-step hydrothermal synthesis of anatase TiO2 nanotubes for efficient photocatalytic CO2 reduction, ACS Omega 7 (2022) 38686–38699.
[40] N. Gilani, J.Vahabzadeh Pasikhani, P.Tafazoli Motie, M. Akbari, Fabrication of quantum Cu(II) nanodot decorated TiO2 nanotubes by the photochemical deposition-assisted hydrothermal method: study catalytic activity in hydrogen generation, Desalin. Water Treat. 139 (2019) 145–155.
[41] L. Jiao, H. Xiao, Q. Wang, J. Sun, Thermal degradation characteristics of rigid polyurethane foam and the volatile products analysis with TG-FTIR-MS, Polym. Degrad. Stab. 98 (2013) 2687–2696.
[42] N. Rastegarfar, R. Behrooz, M. Barikani, Characterization of polyurethane foams prepared from liquefied sawdust by crude glycerol and polyethylene glycol, J. Polym. Res. 25 (2018) 154.
[43] P.M.A. Ebrahimian Pirbazari, B. Fakhari Kisomi, Co/TiO2 nanoparticles: preparation, characterization and its application for photocatalytic degradation of methylene blue, Desalin. Water Treat. 63 (2017) 283–292.
[44] Y. Ding, C. Zhang, W. Liao, J. Peng, Mechanical and electrochemical properties of TiO2 modified polyurethane nanofibers, Appl. Phys. A 129 (2023) 162.
[45] E. Hajialilou, H. Asgharzadeh, S. Khameneh, Asl, TiO2/rGO/Cu2O ternary hybrid for high-performance photoelectrochemical applications, Appl. Surf. Sci. 544 (2021) 148832.
[46] W. Gao, Y. Li, J. Zhao, Z. Zhang, W. Tang, J. Wang, Z. Wu, Photocatalytic degradation of methylene blue from aqueous solutions by rGO/TiO2 nanocomposites, Water, Air, Soil Pollut. 234 (2023) 437.
[47] J. Rashid, S. Saleem, S.U. Awan, A. Iqbal, R. Kumar, M.A. Barakat, M. Arshad, M. Zaheer, M. Rafique, M. Awad, Stabilized fabrication of anatase-TiO2/FeS2 (pyrite) semiconductor composite nanocrystals for enhanced solar light-mediated photocatalytic degradation of methylene blue, RSC Adv. 8 (2018) 11935–11945.
[48] Z. Cui, Ssa Marcelle, M. Zhao, J. Wu, X. Liu, J. Si, Q. Wang, Thermoplastic polyurethane/titania/polydopamine(TPU/TiO2/PDA) 3-D porous composite foam with outstanding oil/water separation performance and photocatalytic dye degradation, Adv. Compos. Hybrid. Mater. 5 (2022) 2801–2816.

[49] Y. Wang, W. Li, C. Li, B. Zhou, Y. Zhou, L. Jiang, S. Wen, F. Zhou, Fabrication of ultra-high working range strain sensor using carboxyl CNTs coated electrospun TPU assisted with dopamine, Appl. Surf. Sci. 566 (2021) 150705.
[50] M. Smith, L. Scudiero, J. Espinal, J.-S. McEwen, M. Garcia-Perez, Improving the deconvolution and interpretation of XPS spectra from chars by ab initio calculations, Carbon 110 (2016) 155–171.
[51] S.D. Delekar, A.G. Dhodamani, K.V. More, T.D. Dongale, R.K. Kamat, S.F. A. Acquah, N.S. Dalal, D.K. Panda, Structural and optical properties of nanocrystalline TiO2 with multiwalled carbon nanotubes and its photovoltaic studies using Ru(II) sensitizers, ACS Omega 3 (2018) 2743–2756.
[52] R. Jonathan, S.U. Rehman, F. Cao, H. Xu, X. Ma, J. Wang, Y. Liu, Y. Niu, X. Jian, N. Mahmood, Low-cost and large-scale preparation of ultrafine TiO2@C hybrids for high-performance degradation of methyl orange and formaldehyde under visible light, 12 (2023).
[53] M. Xing, F. Shen, B. Qiu, J. Zhang, Highly-dispersed Boron-doped Graphene Nanosheets Loaded with TiO2 Nanoparticles for Enhancing CO2 Photoreduction, Sci. Rep. 4 (2014) 6341.
[54] E. Carrasco, M. Oujja, M. Sanz, J.F. Marco, M. Castillejo, X-ray and ion irradiation effects on azurite, malachite and alizarin pictorial models, Microchem. J. 137 (2018) 381–391.
[55] X. Qin, L. Ji, A. Zhu, Construction of rutile/anatase Ohmic heterojunction of TiO2/Ti3C2 with robust built-in electric field for boosting photocatalytic organic pollutant and hydrogen evolution, Appl. Surf. Sci. 652 (2024) 159338.
[56] Y. Yang, S.-H. Liao, W. Shi, Y. Wu, R. Zhang, S.J.R.A. Leng, Nitrogen-doped TiO2 (B) nanorods as high-performance anode materials for rechargeable sodium-ion batteries 7 (2017) 10885–10890.
[57] N. Li, D. Geng, J. Zhou, Ag and Cu nanoparticles synergistically enhance photocatalytic CO2 reduction activity of B phase TiO2, Catal. Lett. 152 (2022) 124–138.
[58] D. Li, H. Song, X. Meng, T. Shen, J. Sun, W. Han, X. WangEffects of particle size on the structure and photocatalytic performance by alkali-treated TiO2, 10 (2020) 546..
[59] J.V. Pasikhani, B.G. Aliabadi, N. Gilani, A.E. Pirbazari, Construction of NiO and Ti3 + self-doped TNTs thin film as a high quantum yield p-n type heterojunction via a novel photoelectrodeposition-assisted anodization method, J. Photochem. Photobiol. A: Chem. 418 (2021) 113433.
[60] X. Deng, H. Zhang, Q. Ma, Y. Cui, X. Cheng, X. Li, M. Xie, Q. Cheng, Fabrication of p-NiO/n-TiO2 nano-tube arrays photoelectrode and its enhanced photocatalytic performance for degradation of 4-chlorphenol, Sep. Purif. Technol. 186 (2017) 1–9.
[61] M. Zulfiqar, S. Chowdhury, A.A. Omar, Hydrothermal synthesis of multiwalled TiO2 nanotubes and its photocatalytic activities for Orange II removal, Sep. Sci. Technol. 53 (2018) 1412–1422.
[62] Z. Liu, Q. Zhang, L.-C. Qin, Reduction in the electronic band gap of titanium oxide nanotubes, Solid State Commun. 141 (2007) 168–171.
[63] T. Peng, S. Ray, S.S. Veeravalli, J.A. Lalman, F. Arefi-Khonsari, The role of hydrothermal conditions in determining 1D TiO2 nanomaterials bandgap energies and crystal phases, Mater. Res. Bull. 105 (2018) 104–113.
[64] M. Thommes, K. Kaneko, A.V. Neimark, J.P. Olivier, F. Rodriguez-Reinoso, J. Rouquerol, K.S.W. Sing, Physisorption of gases, with special reference to the evaluation of surface area and pore size distribution (IUPAC Technical Report), 87 (2015) 1051-1069.
[65] A.H. Zaki, S. Adel, M.M. Abd El-hafiez, A.A. Abdel-Khalek, Improved production of titanate nanotubes by hydrothermal method for adsorption of organic dyes, Beni-Suef Univ. J. Basic Appl. Sci. 10 (2021) 86.
[66] S. Rashad, A.H. Zaki, A.A. Farghali, Morphological effect of titanate nanostructures on the photocatalytic degradation of crystal violet, Nanomater. Nanotechnol. 9 (2019), 1847980418821778.
[67] Z. Zhang, L. Zhang, Z. Huang, Y. Xu, Q. Zhao, H. Wang, M. Shi, X. Li, K. Jiang, D. Wu, "Floating catalytic foam" with prominent heat-induced convection for the effective photocatalytic removal of antibiotics, J. Hazard. Mater. 463 (2024) 132879.
[68] S. Zhang, R. Wang, K. Wang, M. Wang, Z. He, H. Chen, S.-H. Ho, Aeration-free in situ fenton-like reaction: specific adsorption and activation of oxygen on heterophase oxygen vacancies, Environ. Sci. Technol. 58 (2024) 1921–1933.
[69] L. Ren, W. Zhou, L. Wang, K. Lin, Y. Xu, J. Wu, Y. Xie, H. Fu, All-in-one self-floating porous foams as robust heat-blocking layers for efficient photothermal conversion and solar desalination, Sci. Bull. 68 (2023) 2760–2768.
[70] A. Sabir, T.A. Sherazi, Q. Xu, Porous polymer supported Ag-TiO2 as green photocatalyst for degradation of methyl orange, Surf. Interfaces 26 (2021) 101318.
[71] A. Gordanshekan, S. Arabian, A.R. Solaimany Nazar, M. Farhadian, S. Tangestaninejad, A comprehensive comparison of green Bi2WO6/g-C3N4 and Bi2WO6/TiO2 S-scheme heterojunctions for photocatalytic adsorption/degradation of cefixime: artificial neural network, degradation pathway, and toxicity estimation, Chem. Eng. J. 451 (2023) 139067.
[72] R. Ji, Z. Zhang, L. Tian, L. Jin, Q. Xu, J. Lu, Z- scheme heterojunction of BiOI nanosheets grown in situ on NH2-UiO-66 crystals with rapid degradation of BPA in real water, Chem. Eng. J. 453 (2023) 139897.
[73] Q. Zhou, L. Luo, L. Xia, C. Cha, F. Jiang, H. Wang, J. Dai, L. Shu, Persulfate enhanced removal of bisphenol A by copper oxide/reduced graphene oxide foam: influencing factors, mechanism and degradation pathway, Chemosphere 340 (2023) 139786.
[74] S. Krishnan, A.V. Karim, A. Shriwastav, Visible light responsive Cu-N/TiO2 nanoparticles for the photocatalytic degradation of bisphenol A, Water Sci. Technol. 86 (2022) 1527–1539.
[75] R.-a Doong, C.-w Tsai, Synergistic effect of Cu adsorption on the enhanced photocatalytic degradation of bisphenol A by TiO2/titanate nanotubes composites, J. Taiwan Inst. Chem. Eng. 57 (2015) 69–76.